
MixACM: Mixup-Based Robustness Transfer via Distillation of Activated Channel Maps

Muhammad Awais^{1,2*†}, Fengwei Zhou^{1*}, Chuanlong Xie^{1*}, Jiawei Li¹,
Sung-Ho Bae^{2‡}, Zhenguo Li¹

¹ Huawei Noah's Ark Lab

² Department of Computer Science, Kyung-Hee University, South Korea
awais@khu.ac.kr, {zhoufengwei, xie.chuanlong, li.jiawei}@huawei.com,
shbae@khu.ac.kr, li.zhenguo@huawei.com

Abstract

Deep neural networks are susceptible to adversarially crafted, small and imperceptible changes in the natural inputs. The most effective defense mechanism against these examples is adversarial training which constructs adversarial examples during training by iterative maximization of loss. The model is then trained to minimize the loss on these constructed examples. This min-max optimization requires more data, larger capacity models, and additional computing resources. It also degrades the standard generalization performance of a model. Can we achieve robustness more efficiently? In this work, we explore this question from the perspective of knowledge transfer. First, we theoretically show the transferability of robustness from an adversarially trained teacher model to a student model with the help of mixup augmentation. Second, we propose a novel robustness transfer method called Mixup-Based Activated Channel Maps (MixACM) Transfer. MixACM transfers robustness from a robust teacher to a student by matching activated channel maps generated without expensive adversarial perturbations. Finally, extensive experiments on multiple datasets and different learning scenarios show our method can transfer robustness while also improving generalization on natural images.

1 Introduction

Deep learning models have achieved impressive performance on a wide variety of challenging tasks such as image recognition, natural language generation, game playing, etc. However, these models are susceptible to even small changes in the input space. It is possible to craft tiny changes in the input such that a model classifies unaltered input correctly but classifies the same input incorrectly after small and visually imperceptible perturbations [72, 28]. These altered inputs are known as adversarial examples, and this vulnerability of the state-of-the-art models has raised serious concerns [42, 59, 10, 48].

Many defense mechanisms have been proposed to train deep models to be robust against such adversarial perturbations. These techniques include defensive distillation [58], gradient regularization [30, 59, 63], model compression [21, 46], activation pruning [23, 60], adversarial training [50], etc. Among them, Adversarial Training (AT) is one general strategy that is the most effective [4].

*Equal Contribution.

†This work was carried out at Huawei Noah's Ark Lab. The webpage for the project is available at: awais-rauf.github.io/MixACM

‡Corresponding Author.

In general, adversarial training is a kind of data augmentation technique that trains a model on examples augmented with adversarial changes [50]. The adversarial training consists of an inner, iterative maximization loop to augment natural examples with adversarial perturbations, and an outer minimization loop similar to normal training. Many different methods have been introduced to improve robustness [77, 15, 53, 92, 80, 67, 95, 79, 7, 82, 40, 45, 57], but all of them are fundamentally based on the principle of training on adversarially augmented examples.

Adversarial training is more challenging compared with normal training. Better robust generalization requires larger capacity models [50, 54, 81]. Even over-parameterized models that can easily fit data for normal training [93] may have insufficient capacity to fit adversarially augmented data [98]. The sample complexity of adversarial training can be significantly higher than normal training, and it requires more labeled [65] or unlabeled data [77, 15, 53, 92]. The inner maximization for the generation of adversarial perturbations for adversarial training is significantly more expensive computationally as it requires iterative gradient steps with respect to the inputs (e.g., adversarial training takes $\sim 7x$ more time compared with normal training). Adversarial training also degrades the performance of a model on natural examples significantly [54, 95].

Can we attain robustness more efficiently, i.e., with less data, small capacity models, without extra back-propagation steps, and at no significant sacrifice of clean accuracy? For normal training, knowledge transfer is one possible paradigm for the efficient training of deep neural networks. In normal knowledge transfer, a pre-trained teacher model is leveraged to efficiently train a student model on the same or similar dataset [71]. However, knowledge transfer methods are designed to transfer features related to normal generalization which may be at odds with robustness [75, 39]. A recent line of work has explored transferring or distilling robustness from pre-trained models [33, 68, 26, 16]. Although these techniques are effective, they also require extra gradient computation and may not work in some cases.

In this work, we argue that a better approach for robustness transfer is to distill intermediate features of a robust teacher, generated on mixup examples. Our proposed approach does not require any additional gradient computation and works well with smaller models and fewer data samples. It can also effectively transfer robustness across models and datasets.

We begin with the theoretical analysis and show that adversarial loss of a student model can be bounded with two terms: natural loss and distance between the student and teacher model on mixup examples. To minimize the distance between robust teacher and student, we proposed a new distillation method. Our proposed distillation method is based on channel-wise activation analysis of robustness by Bai et al. [7] and other studies showing that adversarially trained models learn fundamentally different features [39, 75, 100].

Channels of a convolutional neural network learn different disentangled representations which, when combined, describe specific semantic concepts [8]. Samples of different classes activate different channels for an intermediate layer. However, adversarial examples make these channels activate more uniformly thereby destroying class-related information. Adversarial training solves this issue by forcing a similar channel-activation pattern for normal and adversarial examples [7]. Our proposed distillation method generates activated channel maps from a robust teacher which has already learned robust channel-activation patterns. The student, then, is forced to match these activated channel maps.

We have conducted extensive experiments to show the effectiveness of our method using various datasets and under different learning settings. We start by exhibiting the ability of our method to transfer robustness without requiring adversarial examples. We then show that our method can distill robustness from large pre-trained models to smaller models and it can transfer robustness across datasets. We also show that our method is capable to robustify a model even with a small number of examples. Concisely, our contributions are as follows:

1. We show that adversarial loss of a student model can be bounded with the distance between robust teacher and student model on mixup examples.
2. We propose a new method to transfer robustness from the intermediate features of robust pre-trained models.
3. We have demonstrated effectiveness of our method with experiments on CIFAR-10, CIFAR-100, and ImageNet datasets. We showed that MixACM can achieve adversarial robustness comparable to the state-of-the-art methods without generating adversarial examples. Our method also improves clean accuracy significantly.

2 Related Work

Adversarial Training and Robust Features. Adversarial attacks are considered to be a security concern [9, 72, 28, 14], and many methods have been proposed to defend against such attacks [30, 28, 58, 31, 59, 74, 50, 12, 44, 63, 21, 46, 23, 60]. Adversarial training [50] is the most effective defense [4] among these methods. The fundamental principle of adversarial training is to generate adversarial perturbation during training by doing iterative back-propagation w.r.t. input. The model is then trained on these perturbed examples. Building upon this principle, different aspects of adversarial training have extensively been studied, e.g., effect of large unlabeled data [77, 15, 92], theoretical aspects to improve the trade-off between accuracy and robustness [95], improving parts of adversarial training for better robustness [79, 82, 57, 7, 29], making adversarial training fast [53, 67, 80, 1], pruning with adversarial training [88, 66], adversarial training with unlabeled data [40], etc. Our work is different from these methods as our main concern is robustness transfer without generating adversarial perturbations. Another line of work studied the effects of adversarial training and showed that adversarial training learns ‘fundamentally different’ [54] features compared with normal training [39, 87, 101]. Our method is motivated by these studies and is designed to leverage these robust features.

Knowledge and Robustness Transfer. Knowledge transfer is training a student model more efficiently on a dataset with the help of a teacher model trained on a similar or related dataset [71]. Many different settings have been explored to achieve this objective by using soft labels produced by teacher [11, 36], knowledge learned by intermediate layers of teacher also called feature distillation [62, 90, 38, 89, 76, 41, 69, 35, 34, 73], or matching input gradients [90, 71]. However, the main objective of these knowledge transfer methods is improving the generalization on natural, unperturbed images. Our work is fundamentally different from these works as we want to transfer robustness.

Our work is motivated by [33, 68, 26, 16, 6] showing transferability of robustness. Hendrycks et al. [33] showed that robust features learned on large datasets like ImageNet can improve adversarial training. Shafahi et al. [67] showed that robust pre-trained models can act as feature extractors in transfer learning. These two methods are limited in application as pre-trained models are used as backbone models. In [26], the authors showed that the robustness can be distilled more efficiently from a large pre-trained teacher model to a smaller student model by using the teacher-produced class scores on adversarial examples. Compared with [26], our method does not require any adversarial training. In [16], the distillation is performed by matching the gradient of the teacher and student, requiring fine-tuning teacher on target dataset and back-propagation to get gradients of the teacher and student w.r.t. inputs and training of a discriminator. Compared with [16], our proposed method does not require any back-propagation steps in addition to those carried out in normal training.

Activation and Robustness. Many works have explored the role of activations in the robustness from different angles, such as modifying output of intermediate layers to improve adversarial training [83, 23, 49, 52, 85], using different activation functions [60, 78, 86, 29, 56, 7, 5] or interpretation of what is learned by adversarial training with activations [87, 7]. However, we leveraged activations to transfer robustness. Our distillation method is inspired by the channel-wise analysis of robustness proposed by Bai et al. [7].

Mixup Augmentation and Robustness. Mixup augmentation was introduced to improve the generalization however, it also improved performance against one-step adversarial attacks [96]. This motivated many mixup-based adversarial defense methods, e.g., Pang et al. [55], Lee et al. [43], Archambault et al. [3], Bunk et al. [13], Chen et al. [17]. These defense methods primarily improve adversarial training by mixup. Our work, however, is different as we explore the role of the mixup in robustness transfer from both theoretical and algorithmic perspectives. Our theoretical work is based on [99] that showed a connection between mixup and robustness theoretically. Goldblum et al. [26] also briefly empirically explored the effect of some augmentation methods on robustness transfer.

3 Setup

We consider task of mapping input $x \in \mathcal{X} \subseteq \mathbb{R}^d$ to label $y \in \mathcal{Y} = \{1, 2, \dots, K\}$. Given the training data $\mathcal{D} = \{(x_1, y_1), \dots, (x_n, y_n)\}$, the goal is to learn a classifier $f : \mathcal{X} \rightarrow \mathbb{R}^k$ from a hypothesis space \mathcal{F} . Let $L(f(x), y)$ be the loss function that measures that how poorly the classifier $f(x)$

predicts the label y . Suppose f can be decomposed into $g \circ h$, where $h \in \mathcal{H}$ is a feature extractor and $g \in \mathcal{G}$ stands for the classifier on top of feature extractor.

Adversarial Augmentation: Adversarial training augments natural examples with adversarial perturbations which are attained by maximizing the loss, i.e., $\tilde{x} = x + \delta$ where $\delta = \arg \max_{\|\delta'\|_p \leq \epsilon} L(f(x + \delta'), y)$. Here $\|\cdot\|_p$ stands for L_p norm. Throughout this paper, we take $p = \infty$. We denote the adversarial loss [50] as:

$$\tilde{\mathcal{L}}(f, \mathcal{D}) = \frac{1}{n} \sum_{i=1}^n \max_{\|\delta\|_\infty \leq \epsilon} L(f(x_i + \delta), y_i),$$

where ϵ is the perturbation budget that governs the adversarial robustness of the model.

Mixup Augmentation: Mixup constructs virtual examples by linearly combining two examples [55]: $\tilde{x}_{ij}(\lambda) = \lambda x_i + (1 - \lambda)x_j$, and $\tilde{y}_{ij}(\lambda) = \lambda y_i + (1 - \lambda)y_j$, where $\lambda \in [0, 1]$ follows the distribution P_λ . The mixup loss is

$$\mathcal{L}_{mix}(f, \mathcal{D}) = \frac{1}{n^2} \sum_{i=1}^n \sum_{j=1}^n \mathbb{E}_{\lambda \sim P_\lambda} [L(f(\tilde{x}_{ij}(\lambda)), \tilde{y}_{ij}(\lambda))].$$

4 Analysis: How to Transfer Robustness?

In this section, we provide an analysis on how to transfer robustness with knowledge distillation and mixup augmentation. We first explore this problem from a theoretical perspective and show that student's adversarial loss can be decomposed into the sum of the teacher's adversarial loss and the distillation loss. Furthermore, these two loss functions can be approximated by mixup-based augmentation. We then discuss how we can design a distillation loss that distills robustness from the intermediate features of a robust model.

4.1 Theoretical Analysis

Robustness Transfer. We give a generalization bound for the robust test error via distillation. Different to the classical bound, we compress the hypothetical space \mathcal{F} into a smaller space derived by the teacher feature extractor. Hsu et al. [37] points out that the distillation helps to derive a fine-grained analysis for the prediction risk and avoid getting a vacuous generalization bound. Therefore, we take the following theorem as a starting point to derive robustness transfer. We consider the loss function $L(f(x), y) = 1 - \phi_\gamma(f(x), y)$, where ϕ_γ is the softmax function with temperature $\gamma > 0$:

$$\phi_\gamma(f(x), y) = \frac{\exp(f(x)_y/\gamma)}{\sum_{k=1}^K \exp(f(x)_k/\gamma)}.$$

Theorem 4.1. *Let the temperature $\gamma > 0$ be given. Then, with probability $1 - \delta$, for any $f \in \mathcal{F}$,*

$$\mathbb{E} \left[\max_{\|\delta\|_\infty \leq \epsilon} \mathbb{I}\{\hat{y}(x + \delta) \neq y\} \right] \leq 2\tilde{\mathcal{L}}(f, \mathcal{D}) + \frac{8}{\gamma} \tilde{\mathcal{L}}_{dis}(f, \mathcal{D}) + 4\mathfrak{R}_S(\Psi_T) + \frac{16}{n} + 6\sqrt{\frac{2/\delta}{2n}}, \quad (1)$$

where \mathfrak{R}_S is the Rademacher complexity, $\Psi_T = \{\max_{\|\delta\|_\infty < \epsilon} L(g \circ h^T(x + \delta), y), g \in \mathcal{G}\}$ and

$$\tilde{\mathcal{L}}_{dis}(f, \mathcal{D}) = \frac{1}{n} \inf_{g \in \mathcal{G}} \sum_{i=1}^n \max_{\|\delta\|_\infty < \epsilon} |f(x_i + \delta) - g \circ h^T(x_i + \delta)|.$$

On the right hand side of (1), two terms depend on the classifier f , i.e., the adversarial loss $\tilde{\mathcal{L}}(f, \mathcal{D})$ and the distillation loss $\tilde{\mathcal{L}}_{dis}(f, \mathcal{D})$. Thus, we can minimize $2\tilde{\mathcal{L}}(f, \mathcal{D}) + 8\tilde{\mathcal{L}}_{dis}(f, \mathcal{D})/\gamma$ to find a classifier with small robust test error. Note that the loss function L is bound above by the cross-entropy loss. So $\tilde{\mathcal{L}}(f, \mathcal{D})$ can be replaced with a common-used adversarial loss based on cross-entropy.

Adversarial Robustness, Transfer and Mixup. However, solving the maximization problem for δ is time-consuming, which is a severe problem in adversarial training especially for large models. For binary classification task with logistic loss function, Zhang et al. [99] proved that $\mathcal{L}(f, \mathcal{D})$ can be

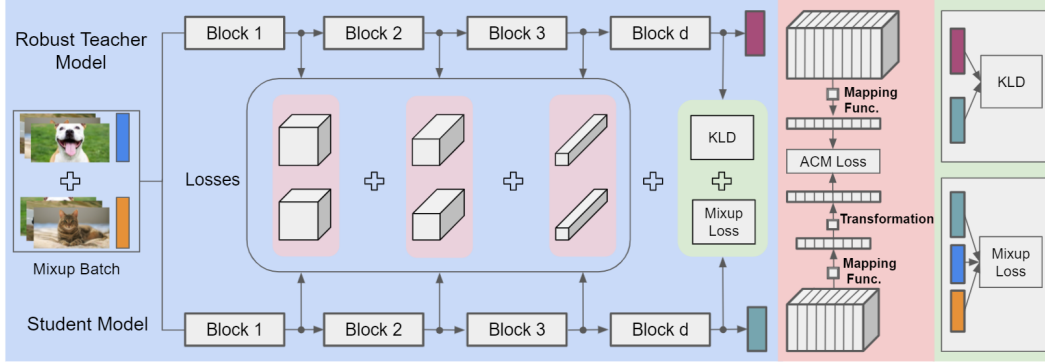


Figure 1: **Overview of our approach.** The mixup augmented examples are passed through a robust teacher and a student to get intermediate features. These features are then passed through a mapping function to get activated channel maps. The student mimics the activated channel maps of robust teacher by minimizing ACM loss. The student model also minimizes the standard KLD and Mixup loss.

bounded above by $\mathcal{L}_{mix}(f, \mathcal{D})$. In addition, the distillation loss that measures the distance between the student model and the teacher model also considers the worst-case δ . In our algorithm, we use the KL divergence or Euclidean distance and mixup sample to design the distillation loss. Inspired by the Theorem 3.3 in [99], we present the following example to illustrate the rationality behind our design.

Theorem 4.2. *Suppose that $\mathcal{Y} = \{0, 1\}$ and L is the logistic loss. Let f be a fully connected neural network with ReLU activation function or max-pooling. Suppose a learnt teacher model f^T with the same network structure is given. Denote $\mathcal{D}_{dis} = \{(x_i, f^T(x_i)), i = 1, \dots, n\}$. Under certain assumptions, we have for any positive scalar α ,*

$$\tilde{\mathcal{L}}(f, \mathcal{D}) + \alpha \tilde{\mathcal{L}}(f, \mathcal{D}_{dis}) \leq \mathcal{L}_{mix}(f, \mathcal{D}) + \alpha \mathcal{L}_{mix}(f, \mathcal{D}_{dis}).$$

This result shows that both the adversarial loss and the distillation loss can be bounded above by their mixup loss. Please see Appendix.B for more details and complete proof. Here the distillation loss is formulated by the prediction accuracy for pseudo-labels generated by a learnt teacher model, which is also considered by [15].

4.2 Considerations for Algorithmic Design

In order to transfer robustness, our theoretical analysis suggests minimizing the distance between teacher and student on mixup examples. However, as observed by Goldblum et al. [26] and our experiments in Section 6, minimization of KL-Divergence between the outputs of teacher and student models is not enough. How can we reduce the gap between the teacher and student more effectively? Based on previous work [24, 87, 7], we hypothesize that the gap between latent space of robust teacher and student is large and it requires distillation from intermediate features.

To reduce the distance between the latent spaces of robust teacher and student, we get inspiration from recent channel-based analysis of robustness [7] and works on the interpretation of what is learned by robust models [54, 39, 87]. Specifically, we consider convolution channels of CNNs to be fundamental learning blocks: each channel learns class-specific patterns and the output of the model is a combination of these basic patterns. As noted by [39], these basic blocks learn both robust and non-robust features with natural training. Adversarial examples amplify non-robust features while suppressing the robust features, e.g., adversarial examples frequently activate channels that are rarely activated by natural examples [7]. Adversarial training works by suppressing non-robust channels and making the activation frequency of natural and adversarial examples similar.

Motivated by this analysis, we propose Activated Channel Map (ACM) transfer loss. Our method extracts the activated channel maps of the robust model’s intermediate features on mixup examples. The student is then forced to mimic these maps. Specifically, we consider the maximum value of each channel as a proxy for the extent of how activated a channel is: a channel is less activated if it has a smaller maximum value and more activated if it has a high maximum value. We then make the student match the normalized activation map of the teacher. And, further analysis of our method is presented in the supplementary material. We present the core of our method in the next section.

5 Methodology

5.1 Activated Channels Maps (ACM) Transfer Loss

In this section, we introduce our Mixup-Based Robustness Transfer method. As discussed above, the method aims to transfer robustness from a robust teacher model f^T to a student model f^S via matching activated channel maps of a robust teacher on mixup augmented examples. An overview of our method is given in Figure 1.

The purpose of robust teacher is to supervise the student’s focus on robust features. This is achieved by matching activated channel maps of teacher and student. The activated channel maps of a model is extracted as follows: given i -th block activations \mathcal{A}_i (output of i -th layer), we apply a function $g_c : \mathbb{R}^{B \times C \times H \times W} \rightarrow \mathbb{R}^{B \times C \times 1 \times 1}$ to get the activated channel map $a_i = g_c(\mathcal{A}_i)$, as illustrated in Figure 2.

The activated channel map of student and teacher may differ in scale. The contribution of each channel in the final output, on the other hand, depends only on the relative value compared with other channels. Therefore, we first normalize this map. To force the student to mimic the teacher’s activated channel maps, we use ℓ_2 distance between the normalized activated channel maps of teacher and student. For i -th layer, we can define ACM loss as:

$$\mathcal{L}_{acm_i}(\mathcal{A}_i^T, \mathcal{A}_i^S) = \left\| \frac{a_i^T}{\|a_i^T\|_2} - \frac{a_i^S}{\|a_i^S\|_2} \right\|_2^2.$$

We minimize this distance at the end of each block of the models. A block is a set of convolution layers grouped like residual blocks in ResNets [32]. For a student and teacher model with d such blocks, the total ACM loss becomes as follows: $\mathcal{L}_{acm}(x; f^T, f^S) = \sum_{i=0}^d \mathcal{L}_{acm_i}(f^T(x)_i, f^S(x)_i)$, where $f(x)_i$ represents output of the model at i -th block.

Mapping Function (g_c): The aim of activated channel map function (g_c) is to extract a map of least to most activated channels. For this purpose, we used maximum value of each channel: $g_c(x) = \max_i x_i \forall i \in \{0, \dots, c_l\}$, where c_l is number of channels in l -th layer.

5.2 Transferring Robustness with Different Feature Sizes

Our method extracts a scalar value corresponding to each channel in a layer. Until now, we assume that the teacher and student have the same number of channels. For this case, we only need the g_c mapping function. To accomplish knowledge transfer across models with a different number of channels, we need to apply transformation either on a teacher or student’s activated channel maps. We experimented with two transformations: adaptive pooling and affine transformation.

Adaptive Pooling: Pooling is used in most CNN architectures to reduce the size of feature vectors and gain invariance to small transformations of the input. The pooling layer works by dividing the input into patches and taking an average or maximum value over these patches. By changing the size of these patches, pooling can also be used for up-sampling. Pooling operation can be described as follows: $y[p] = \max_{q \in \Omega(p)} x[q]$, where Ω represents a patch or neighbourhood of $x[p]$. We use PyTorch implementation of 1d adaptive maximum pooling to either down or up-sample teacher or student output.

Affine Transformation: We can also use the learning function to convert the input size to output size. For this, we use a fully connected layer. Based on our ablation studies described in supplementary material, we use adaptive pooling as a default in our method.

5.3 KL Divergence Loss with Soft Labels

Soft labels have shown to be useful for adversarial robustness by Pang et al. [56]. Therefore, for distillation on the same dataset (e.g., where teacher and student have the same classification layer), we minimize the KL divergence between the logits provided by teacher and student following [36, 26]. The KLD loss becomes as follows: $\mathcal{L}_{kld}(x; f^T, f^S) = \gamma^2 KL(y^T(\gamma), y^S(\gamma))$, where γ is

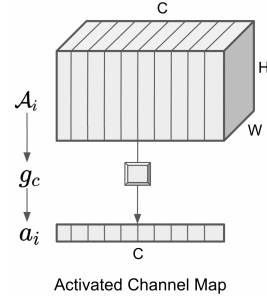


Figure 2: Mapping function g_c is applied channel-wise to get the Activated Channel Maps (ACM).

Table 1: **Detailed Comparison.** CIFAR-10 test accuracy and robustness comparison under two different ℓ_∞ attacks of magnitude $\epsilon = 8/255$. Our method outperforms robustness distillation methods in both accuracy and robustness. It outperforms various existing state-of-the-art robust models in clean accuracy while retaining comparable robustness. All reported values for our method are mean \pm std of five repetitions. B.P. in the table stands for back propagation.

Method	Model	Extra B.P. Steps	Clean Acc.	PGD 100	Auto Attack
AT (Madry et al. [50])	WRN-34-10	✓	87.14	47.04	44.04
LAT (Singh et al. [70])	WRN-34-10	✓	87.80	53.04	49.12
TLA (Mao et al. [51])	WRN-34-10	✓	86.21	50.03	47.41
YOPO (Zhang et al. [94])	WRN-34-10	✓	87.20	47.98	44.83
Free AT (Shafahi et al. [67])	WRN-34-10	✓	86.11	46.19	41.47
TRADES (Zhang et al. [95])	WRN-34-10	✓	84.92	56.43	53.08
MART (Wang et al. [79])	WRN-34-10	✓	83.07	55.57	-
AWP (Wu et al. [82])	WRN-34-10	✓	85.36	59.12	56.17
FAT (Zhang et al. [97])	WRN-34-10	✓	84.52	54.36	53.51
Overfitting (Rice et al. [61])	WRN-34-20	✓	85.34	58.00	53.42
BoT TRADES (Pang et al. [56])	WRN-34-20	✓	86.43	54.39	54.39
Adv. Pretraining (Hendrycks et al. [33])	WRN-28-10	✓	87.10	57.40	54.92
IGAM (Chan et al. [16])	WRN-34-10	✓	88.70	43.00	-
RKD (Goldblum et al. [27])	WRN-34-10	×	89.38	0.21	0
Ours (w/o Mixup)	WRN-34-10	×	91.17 \pm 0.06	49.53 \pm 1.44	47.38 \pm 1.51
Ours (w/ Mixup)	WRN-34-10	×	90.76 \pm 0.05	56.65 \pm 0.93	53.93 \pm 0.77

the temperature parameter, and $y(\gamma)$ is output logits of a model normalized by temperature parameter as used by Hinton et al. [36]. We omit this loss term when transferring from one dataset to another.

5.4 Mixup Fueled Distillation

Our theoretical analysis suggest minimizing distance between teacher and student with mixup examples. To this end, we use mixup to linearly combine inputs and outputs and minimize loss on these inputs. The final training objective for the student is as follows:

$$\min_{f^S} \mathbb{E}_{(x,y) \sim \mathcal{D}} \mathbb{E}_{\lambda \sim P_\lambda} [(1 - \alpha_{kld}) \mathcal{L}_{mix} + \alpha_{kld} \mathcal{L}_{kld} + \alpha_{acm} \mathcal{L}_{acm}],$$

where α_{kld} and α_{acm} are hyperparameters for corresponding loss terms.

6 Experiments

In this section, we empirically evaluate our method for robustness transfer. We primarily show the effectiveness of our method under three settings: 1) Robustness Transfer in Section 6.1 to demonstrate that our method can transfer robustness from a pre-trained teacher to student without generating adversarial examples; 2) Robustness transfer from larger to smaller models in Section 6.2 to show its effectiveness under distillation settings; and 3) robustness transfer under transfer learning settings, e.g., from one dataset to another dataset and robustness with smaller dataset sizes in Section 6.3.

Evaluation of Robustness: We evaluate MixACM and other methods against standard FGSM and PGD-k as well as the strongest auto-attack by Croce and Hein [19]: a parameter-free adversarial attack designed to give a reliable evaluation of robustness. It is an ensemble of four white and black-box attacks. Apart from these, we also report robustness of our robust models on auto pgd-ce [19], auto pgd-dlr [19], FAB [18] and query-based black-box attack called Square attack [2]. For PGD-k, we use the standard value of step size ($2/255$), and evaluated the model with an increasing number of iterations (k), including an extreme version: PGD-500.

Pre-Trained Robust Models: For CIFAR experiments, we use WideResNet-28-10 and WideResNet-34-20 [91] provided by Gowal et al. [29]. For ImageNet experiments, we use adversarially trained ResNet-50 provided by Salman et al. [64].

Training Details: For CIFAR experiments, we use WideResNet-34-10 [91] as student model following [16]. All student models for our proposed method are trained without adversarial perturbations.

Table 2: **Comparison on ImageNet.** Results of robustness transfer for large-scale ImageNet dataset with ResNet-50 with two different training settings. Our method has significantly better robustness while also achieving comparable or better clean accuracy although it does not require any additional back-propagation steps.

Method	Train ϵ	Acc.	Test $\epsilon = 2/255$			Train ϵ	Acc.	Test $\epsilon = 4/255$		
			PGD10	PGD50	PGD100			PGD10	PGD50	PGD100
Free-AT [67]	2	64.45	43.52	43.39	43.40	4	60.21	32.77	31.88	31.82
Fast-AT [80]	2	60.90	-	43.46	-	4	55.45	-	30.28	-
Ours	0	59.64	46.03	45.96	45.92	0	59.64	32.70	31.51	31.39
Ours+RA	0	62.05	48.54	48.45	48.44	0	62.05	34.93	33.71	33.63

Table 3: **Distillation Results.** Performance for robustness distillation on CIFAR-10 and CIFAR-100 datasets. The teacher model is WideResNet-28-10 and student model is WideResNet-16-10. Robustness is reported for diverse set of attacks of smagnitude $\epsilon = 8/255$.

Dataset	Method	Acc.	FGSM	PGD 20	PGD 500	APGD CE	APGD DLR	FAB	Square	Auto Attack
CIFAR-10	Natural	93.79	5.34	0	0	0	0	0	0	0
	PGD7-AT	83.90	53.07	47.55	47.36	47.28	44.52	44.89	53.26	44.51
	RKD	88.60	27.37	0.12	0	0	0	0	7.31	0
	Ours w/o mixup	90.47	56.98	40.69	39.69	39.24	36.46	37.21	56.30	36.42
	Ours	89.93	59.48	48.09	47.51	47.31	43.73	44.46	60.20	43.64
CIFAR-100	Natural	76.91	3.17	0	0	0	0	0	0	0
	PGD7-AT	60.29	28.37	24.94	24.75	24.71	21.94	22.16	27.97	21.94
	RKD	67.19	10.27	0.23	0.16	0.04	0	0	3.73	0
	Ours w/o mixup	60.81	30.13	25.38	25.12	24.93	19.51	19.83	29.74	19.50
	Ours	59.35	31.89	28.24	28.20	27.96	22.02	22.26	31.60	22.02

We trained them for 200 epochs, using batch size of 128, a learning rate of 0.1, cosine learning rate scheduler [47], momentum optimizer with weight decay of 0.0005. For our loss, we use $\alpha_{acm} = 5000$. For KD loss, we use temperature value of $\gamma = 10$ and $\alpha_{kld} = 0.95$ and the value for mixup coefficient is $\alpha_{mixup} = 1$ whereas $\lambda \sim \text{Beta}(\alpha_{mixup}, \alpha_{mixup})$ following [96]. ImageNet models are trained for 120 epochs. Additional training details are in the supplementary material.

6.1 Transferring Robustness without Adversarial Examples

CIFAR-10: To show the effectiveness of our method for robustness transfer and compare it with state-of-the-art, we follow settings of [16]: WideResNet-34-10 as a student on CIFAR-10. We compare our method with two kinds of defense methods: general variants of adversarial training and three robustness transfer methods. For our method, the average \pm variance of five runs for our method are shown in Table 1. The robustness of our method is comparable to most state-of-the-arts adversarial training methods while still maintaining significantly higher clean accuracy.

ImageNet: We also consider high-resolution, large-scale ImageNet dataset [22]. This dataset is significantly more challenging for robustness [85, 84]. The results of our method for ResNet-50 student are shown in Table 2. For our method, we show two results: one with only mixup augmentation and one with mixup and random augmentation [20]. We observed that addition of random augmentation further improves the results of our method. Our method outperforms both Free [67] and Fast [80] AT in accuracy and robustness, significantly.

6.2 Robustness Distillation for Model Compression

A benefit of our method is its ability to distill robustness across models. To show this, we conduct two sets of experiments. First, we show robustness distillation from WideResNet-28-10 to WideResNet-16-10 for CIFAR-10 and CIFAR-100 datasets. The results are shown in Table 3. To see the effect of robustness transfer across different models, we also conduct an experiment where we changed the size of the model in terms of depth, the number of channels, or both, e.g., WideResNet-28-10 to WideResNet-16-5. The results are shown in Table 4. Our method works well for both larger-to-smaller

Table 4: **Model Compression.** Comparison of our method with PGD-7 Adversarial Training for accuracy and robustness on various sizes of models. The robustness is reported for ℓ_∞ PGD-20 attack of magnitude $\epsilon = 8/255$. Our method works well for robustness transfer from larger to smaller as well as, for smaller to larger models.

Distill Type	Teacher	Student	Size Ratio	PGD7-AT		Ours	
				Acc.	Rob.	Acc.	Rob.
Depth	WRN-28-10	WRN-16-10	46.92%	83.90	47.55	89.93	48.09
Channel	WRN-28-10	WRN-28-5	25.04%	83.90	47.74	90.26	48.75
Channel	WRN-34-20	WRN-34-10	25.01%	84.30	49.72	87.26	52.83
Depth & Channel	WRN-28-10	WRN-16-5	11.76%	83.51	48.11	88.96	36.95
Depth & Channel	WRN-34-20	WRN-16-10	9.227%	83.90	47.55	86.31	47.18
Tiny network	WRN-28-10	WRN-10-1	0.21%	67.11	38.85	66.65	1.15
Tiny network	WRN-34-20	WRN-10-1	0.04%	67.11	38.85	63.19	3.75
Same network	WRN-28-10	WRN-28-10	100%	84.17	49.23	90.48	54.05
Same network	WRN-34-20	WRN-34-20	100%	84.20	49.11	87.17	53.60
Up Transfer	WRN-28-10	WRN-34-20	505.85%	84.20	49.11	90.67	58.36

Figure 3: Robustness Transfer with Smaller Data. Figure shows robustness and accuracy (%) for the student model trained with different fractions of CIFAR-10 dataset. Our method achieves significantly better clean accuracy and robustness compared with adversarial training. Dotted blue line shows the performance of adversarial training with full data.

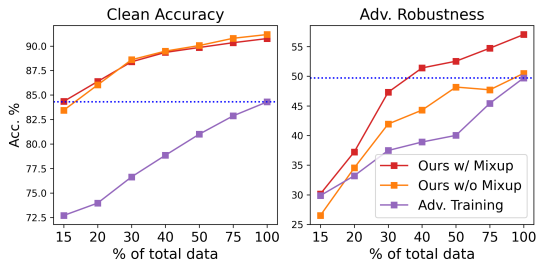


Table 5: Robustness Transfer from ImageNet to CIFAR-100. Teacher model is adversarially trained on ImageNet and student is trained on CIFAR-100. Our method achieves significantly better clean accuracy and better robustness compared with both adversarial training and IGAM [16]. The robustness is reported according to [16] for a fair comparison. Reported results for our method are mean of five repetitions.

Defense	Acc.	FGSM	PGD-k		
			5	10	20
Natural [16]	78.70	7.95	0.13	0.03	0
PGD7-AT [16]	60.40	29.10	29.30	24.30	23.50
IGAM [16]	62.39	34.31	29.59	24.05	21.74
Ours w/o Mixup	68.91	29.09	28.65	21.70	20.27
Ours	65.69	32.09	32.04	25.58	24.14

as well as smaller-to-larger models. However, our method does not perform well when both depth and number of channels are decreased dramatically, e.g., from WideResNet-34-20 to WideResNet-10-1 (student’s size is 0.04% of teacher’s size). To elaborate further, we discuss this in the supplementary material.

6.3 Robust Transfer Learning

To further show the effectiveness of our method, we conduct two sets of experiments under transfer learning settings: transfer learning from one dataset to another dataset and transfer learning with fewer data samples. For first experiment, we follow Hendrycks et al. [33]’s setting: our teacher model is a WideResNet-28-10 trained on ImageNet of size 32×32 and student is a WideResNet-34-10. The results for the CIFAR-100 dataset under these settings are shown in Table 5.

For the second part, we show the effectiveness of our method with fewer data points. To this end, we randomly choose a smaller portion of CIFAR-10 and conducted experiments on this smaller portion of data with our method as well with PGD-7 adversarial training. The results are shown in Figure 3. Our method outperforms adversarial training significantly for both robustness and clean accuracy. Using just 30% of the data, our method can match the robustness and clean accuracy of a robust model trained on all the data.

Table 6: **Ablation Studies:** (a) Impact of different components of our proposed distillation method. We use WideResNet-34-10 as student following Table 1 in the main text. (b) Impact of using different intermediate features on clean accuracy and robustness of student.

(a)						(b)		
	Std. Setting	w/o KD	w/o Mixup	Only ACM	Only KD	Features Used	Acc.	Rob.
Mapping (g_c)	✓	✓	✓	✓		Low-Level (2)	86.36	17.24
Soft Labels	✓		✓		✓	Mid-Level (3)	88.30	39.37
Mixup	✓	✓				High-Level (4)	91.18	33.13
ACM Loss	✓	✓	✓	✓		Low+Mid Level (2+3)	88.15	41.92
						Mid+High Level (3+4)	90.69	52.79
Accuracy	90.76	92.50	91.17	92.87	89.38	First Layer Only (1)	86.00	0.31
Robustness	56.65	52.29	49.53	48.38	0.21	No First Layer (2+3+4)	90.69	56.15
						All Features	90.76	56.65

6.4 Ablation Studies

Effect of Individual Components: To see the effect of individual components of our proposed method, we perform an experiment where we try different settings. The results are shown in Table 6(a). ACM loss alone is sufficient to transfer significant robustness but adding mixup and soft labels improves the transferability. However, the improvement in robustness comes at the cost of clean accuracy. Also, note that only soft labels are not enough to transfer robustness as shown by KD Only column. This is in line with the observations of Goldblum et al. [26].

Role of Intermediate Features: To understand the role of low, mid, and high-level features, we performed experiments on CIFAR-10 by progressively changing blocks used for distillation. For this ablation study, we kept all the standard settings reported in the paper (supplementary material section A.1). Our correspondence of blocks and features is as follows: block 2: low-level features; block 3: mid-level features; block 4: high-level features. Please note that block 1 corresponds to the output of the first layer only. Therefore, we do not call it low-level features.

The results are reported in Table 6 (b). In summary, all level features (low, mid, high level) improve robustness and accuracy. However, mid-level features seem to be more critical for robustness and high-level features for accuracy. For more details, please refer to supplementary material.

Other Ablation Studies: We have conducted several additional ablation studies and discussed them in the supplementary material (Section A). We recapitulate the purpose of these ablation studies here for reference. First, we conducted a study to understand the effect of direct distillation vs. distillation via MixACM. Second, we performed an ablation study to see the effect of three hyperparameters used by our loss (α_{acm} , α_{kld} , γ). Third, we performed a study to see how different transforms ($g_c(\cdot)$) effect the results. Fourth, to see the limitation of our method, we performed an experiment with progressively decreasing the size of student. Finally, we also compared activation maps of a normally trained student, teacher and model trained with our method.

7 Conclusion

In this paper, we have investigated robustness transfer from a theoretical and algorithmic perspective. The general principle behind most successful adversarial defense methods is the generation of adversarial examples during training. However, adversarial training is complicated as it requires more data, larger models, higher compute resources and degrades clean accuracy. We investigated whether we can have robustness more efficiently through robustness transfer. To this end, we first presented a theoretical result bounding adversarial loss of student model with the distance between robust teacher and student on mixup examples. We, then, proposed a novel robustness transfer method that is based on channel-wise analysis of robustness. Our method can achieve significant robustness against challenging and reliable auto-attack as well as other standard attacks while outperforming previous work in terms of clean accuracy. The proposed method also works well for the distillation of robustness to a smaller model, and for transfer learning with fewer data points.

Acknowledgements: Authors are thankful to Ferjad Naem, Dr. Nauman, and anonymous reviewers for their valuable feedback.

References

- [1] Maksym Andriushchenko and Nicolas Flammarion. Understanding and improving fast adversarial training. *Advances in Neural Information Processing Systems*, 33, 2020.
- [2] Maksym Andriushchenko, Francesco Croce, Nicolas Flammarion, and Matthias Hein. Square attack: a query-efficient black-box adversarial attack via random search. In *European Conference on Computer Vision*, pages 484–501. Springer, 2020.
- [3] Guillaume P Archambault, Yongyi Mao, Hongyu Guo, and Richong Zhang. Mixup as directional adversarial training. *arXiv preprint arXiv:1906.06875*, 2019.
- [4] Anish Athalye, Nicholas Carlini, and David Wagner. Obfuscated gradients give a false sense of security: Circumventing defenses to adversarial examples. In *International Conference on Machine Learning*, pages 274–283. PMLR, 2018.
- [5] Muhammad Awais, Fahad Shamshad, and Sung-Ho Bae. Towards an adversarially robust normalization approach. *arXiv preprint arXiv:2006.11007*, 2020.
- [6] Muhammad Awais, Fengwei Zhou, Hang Xu, Lanqing Hong, Ping Luo, Sung-Ho Bae, and Zhenguo Li. Adversarial robustness for unsupervised domain adaptation. In *Proceedings of the IEEE/CVF International Conference on Computer Vision*, pages 8568–8577, 2021.
- [7] Yang Bai, Yuyuan Zeng, Yong Jiang, Shu-Tao Xia, Xingjun Ma, and Yisen Wang. Improving adversarial robustness via channel-wise activation suppressing. *arXiv preprint arXiv:2103.08307*, 2021.
- [8] David Bau, Jun-Yan Zhu, Hendrik Strobelt, Agata Lapedriza, Bolei Zhou, and Antonio Torralba. Understanding the role of individual units in a deep neural network. *Proceedings of the National Academy of Sciences*, 2020. ISSN 0027-8424. doi: 10.1073/pnas.1907375117. URL <https://www.pnas.org/content/early/2020/08/31/1907375117>.
- [9] Battista Biggio, Igino Corona, Davide Maiorca, Blaine Nelson, Nedim Šrđić, Pavel Laskov, Giorgio Giacinto, and Fabio Roli. Evasion attacks against machine learning at test time. In *Joint European conference on machine learning and knowledge discovery in databases*, pages 387–402. Springer, 2013.
- [10] Tom B Brown, Dandelion Mané, Aurko Roy, Martín Abadi, and Justin Gilmer. Adversarial patch. *arXiv preprint arXiv:1712.09665*, 2017.
- [11] Cristian Bucilua, Rich Caruana, and Alexandru Niculescu-Mizil. Model compression. In *Proceedings of the 12th ACM SIGKDD international conference on Knowledge discovery and data mining*, pages 535–541, 2006.
- [12] Jacob Buckman, Aurko Roy, Colin Raffel, and Ian Goodfellow. Thermometer encoding: One hot way to resist adversarial examples. In *International Conference on Learning Representations*, 2018.
- [13] Jason Bunk, Srinjoy Chattopadhyay, BS Manjunath, and Shivkumar Chandrasekaran. Adversarially optimized mixup for robust classification. *arXiv preprint arXiv:2103.11589*, 2021.
- [14] Nicholas Carlini and David Wagner. Towards evaluating the robustness of neural networks. In *2017 IEEE symposium on security and privacy (sp)*, pages 39–57. IEEE, 2017.
- [15] Yair Carmon, Aditi Raghunathan, Ludwig Schmidt, Percy Liang, and John C Duchi. Unlabeled data improves adversarial robustness. *arXiv preprint arXiv:1905.13736*, 2019.
- [16] Alvin Chan, Yi Tay, and Yew-Soon Ong. What it thinks is important is important: Robustness transfers through input gradients. In *Proceedings of the IEEE/CVF Conference on Computer Vision and Pattern Recognition*, pages 332–341, 2020.
- [17] Chen Chen, Jingfeng Zhang, Xilie Xu, Tianlei Hu, Gang Niu, Gang Chen, and Masashi Sugiyama. Guided interpolation for adversarial training. *arXiv e-prints*, pages arXiv–2102, 2021.
- [18] Francesco Croce and Matthias Hein. Minimally distorted adversarial examples with a fast adaptive boundary attack. In *International Conference on Machine Learning*, pages 2196–2205. PMLR, 2020.
- [19] Francesco Croce and Matthias Hein. Reliable evaluation of adversarial robustness with an ensemble of diverse parameter-free attacks. In *ICML*, 2020.
- [20] Ekin D Cubuk, Barret Zoph, Jonathon Shlens, and Quoc V Le. Randaugment: Practical automated data augmentation with a reduced search space. In *Proceedings of the IEEE/CVF Conference on Computer Vision and Pattern Recognition Workshops*, pages 702–703, 2020.

- [21] Nilaksh Das, Madhuri Shanbhogue, Shang-Tse Chen, Fred Hohman, Siwei Li, Li Chen, Michael E Kounavis, and Duen Horng Chau. Compression to the rescue: Defending from adversarial attacks across modalities. In *ACM SIGKDD Conference on Knowledge Discovery and Data Mining*, 2018.
- [22] Jia Deng, Wei Dong, Richard Socher, Li-Jia Li, Kai Li, and Li Fei-Fei. Imagenet: A large-scale hierarchical image database. In *2009 IEEE conference on computer vision and pattern recognition*, pages 248–255. Ieee, 2009.
- [23] Guneet S Dhillon, Kamyar Azizzadenesheli, Zachary C Lipton, Jeremy D Bernstein, Jean Kossaifi, Aran Khanna, and Animashree Anandkumar. Stochastic activation pruning for robust adversarial defense. In *International Conference on Learning Representations*, 2018.
- [24] Logan Engstrom, Andrew Ilyas, Shibani Santurkar, Dimitris Tsipras, Brandon Tran, and Aleksander Madry. Adversarial robustness as a prior for learned representations. *arXiv preprint arXiv:1906.00945*, 2019.
- [25] Bolin Gao and Lacra Pavel. On the properties of the softmax function with application in game theory and reinforcement learning. *arXiv preprint arXiv:1704.00805*, 2017.
- [26] Micah Goldblum, Liam Fowl, Soheil Feizi, and Tom Goldstein. Adversarially robust distillation. *Proceedings of the AAAI Conference on Artificial Intelligence*, 2020. doi: 10.1609/aaai.v34i04.5816.
- [27] Micah Goldblum, Liam Fowl, Soheil Feizi, and Tom Goldstein. Adversarially robust distillation. In *Proceedings of the AAAI Conference on Artificial Intelligence*, pages 3996–4003, 2020.
- [28] Ian J Goodfellow, Jonathon Shlens, and Christian Szegedy. Explaining and harnessing adversarial examples. *arXiv preprint arXiv:1412.6572*, 2014.
- [29] Sven Gowal, Chongli Qin, Jonathan Uesato, Timothy Mann, and Pushmeet Kohli. Uncovering the limits of adversarial training against norm-bounded adversarial examples. *arXiv preprint arXiv:2010.03593*, 2020. URL <https://arxiv.org/pdf/2010.03593>.
- [30] Shixiang Gu and Luca Rigazio. Towards deep neural network architectures robust to adversarial examples. *arXiv preprint arXiv:1412.5068*, 2014.
- [31] Chuan Guo, Mayank Rana, Moustapha Cisse, and Laurens Van Der Maaten. Countering adversarial images using input transformations. *arXiv preprint arXiv:1711.00117*, 2017.
- [32] Kaiming He, Xiangyu Zhang, Shaoqing Ren, and Jian Sun. Deep residual learning for image recognition. In *Proceedings of the IEEE conference on computer vision and pattern recognition*, pages 770–778, 2016.
- [33] Dan Hendrycks, Kimin Lee, and Mantas Mazeika. Using pre-training can improve model robustness and uncertainty. *Proceedings of the International Conference on Machine Learning*, 2019.
- [34] Byeongho Heo, Jeesoo Kim, Sangdoo Yun, Hyojin Park, Nojun Kwak, and Jin Young Choi. A comprehensive overhaul of feature distillation. In *Proceedings of the IEEE/CVF International Conference on Computer Vision*, pages 1921–1930, 2019.
- [35] Byeongho Heo, Minsik Lee, Sangdoo Yun, and Jin Young Choi. Knowledge transfer via distillation of activation boundaries formed by hidden neurons. In *Proceedings of the AAAI Conference on Artificial Intelligence*, pages 3779–3787, 2019.
- [36] Geoffrey Hinton, Oriol Vinyals, and Jeff Dean. Distilling the knowledge in a neural network. *arXiv preprint arXiv:1503.02531*, 2015.
- [37] Daniel Hsu, Ziwei Ji, Matus Telgarsky, and Lan Wang. Generalization bounds via distillation. *arXiv preprint arXiv:2104.05641*, 2021.
- [38] Zehao Huang and Naiyan Wang. Like what you like: Knowledge distill via neuron selectivity transfer. *arXiv preprint arXiv:1707.01219*, 2017.
- [39] Andrew Ilyas, Shibani Santurkar, Logan Engstrom, Brandon Tran, and Aleksander Madry. Adversarial examples are not bugs, they are features. *Advances in neural information processing systems*, 32, 2019.
- [40] Minseon Kim, Jihoon Tack, and Sung Ju Hwang. Adversarial self-supervised contrastive learning. *Advances in Neural Information Processing Systems*, 33, 2020.
- [41] Animesh Koratana, Daniel Kang, Peter Bailis, and Matei Zaharia. Lit: Learned intermediate representation training for model compression. In *International Conference on Machine Learning*, pages 3509–3518. PMLR, 2019.

- [42] Alexey Kurakin, Ian Goodfellow, Samy Bengio, et al. Adversarial examples in the physical world, 2016.
- [43] Saehyung Lee, Hyungyu Lee, and Sungroh Yoon. Adversarial vertex mixup: Toward better adversarially robust generalization. In *Proceedings of the IEEE/CVF Conference on Computer Vision and Pattern Recognition*, pages 272–281, 2020.
- [44] Fangzhou Liao, Ming Liang, Yinpeng Dong, Tianyu Pang, Xiaolin Hu, and Jun Zhu. Defense against adversarial attacks using high-level representation guided denoiser. In *Proceedings of the IEEE Conference on Computer Vision and Pattern Recognition*, pages 1778–1787, 2018.
- [45] Wei-An Lin, Chun Pong Lau, Alexander Levine, Rama Chellappa, and Soheil Feizi. Dual manifold adversarial robustness: Defense against lp and non-lp adversarial attacks. *Advances in Neural Information Processing Systems Foundation (NeurIPS)*, 2020.
- [46] Qi Liu, Tao Liu, Zihao Liu, Yanzhi Wang, Yier Jin, and Wujie Wen. Security analysis and enhancement of model compressed deep learning systems under adversarial attacks. In *2018 23rd Asia and South Pacific Design Automation Conference (ASP-DAC)*, pages 721–726. IEEE, 2018.
- [47] Ilya Loshchilov and Frank Hutter. Sgdr: Stochastic gradient descent with warm restarts. *International Conference on Learning Representations*, 10:3, 2017.
- [48] Xingjun Ma, Yuhao Niu, Lin Gu, Yisen Wang, Yitian Zhao, James Bailey, and Feng Lu. Understanding adversarial attacks on deep learning based medical image analysis systems. *Pattern Recognition*, 110: 107332, 2021.
- [49] Divyam Madaan, Jinwoo Shin, and Sung Ju Hwang. Adversarial neural pruning with latent vulnerability suppression. In *International Conference on Machine Learning*, pages 6575–6585. PMLR, 2020.
- [50] Aleksander Madry, Aleksandar Makelov, Ludwig Schmidt, Dimitris Tsipras, and Adrian Vladu. Towards deep learning models resistant to adversarial attacks. *arXiv preprint arXiv:1706.06083*, 2017.
- [51] Chengzhi Mao, Ziyuan Zhong, Junfeng Yang, Carl Vondrick, and Baishakhi Ray. Metric learning for adversarial robustness. *arXiv preprint arXiv:1909.00900*, 2019.
- [52] Aamir Mustafa, Salman H Khan, Munawar Hayat, Roland Goecke, Jianbing Shen, and Ling Shao. Deeply supervised discriminative learning for adversarial defense. *IEEE transactions on pattern analysis and machine intelligence*, 2020.
- [53] Amir Najafi, Shin-ichi Maeda, Masanori Koyama, and Takeru Miyato. Robustness to adversarial perturbations in learning from incomplete data. *arXiv preprint arXiv:1905.13021*, 2019.
- [54] Preetum Nakkiran. Adversarial robustness may be at odds with simplicity. *arXiv preprint arXiv:1901.00532*, 2019.
- [55] Tianyu Pang, Kun Xu, and Jun Zhu. Mixup inference: Better exploiting mixup to defend adversarial attacks. *arXiv preprint arXiv:1909.11515*, 2019.
- [56] Tianyu Pang, Xiao Yang, Yinpeng Dong, Hang Su, and Jun Zhu. Bag of tricks for adversarial training. *arXiv preprint arXiv:2010.00467*, 2020.
- [57] Tianyu Pang, Xiao Yang, Yinpeng Dong, Kun Xu, Jun Zhu, and Hang Su. Boosting adversarial training with hypersphere embedding. *arXiv preprint arXiv:2002.08619*, 2020.
- [58] Nicolas Papernot, Patrick McDaniel, Xi Wu, Somesh Jha, and Ananthram Swami. Distillation as a defense to adversarial perturbations against deep neural networks. In *2016 IEEE symposium on security and privacy (SP)*, pages 582–597. IEEE, 2016.
- [59] Nicolas Papernot, Patrick McDaniel, Ian Goodfellow, Somesh Jha, Z Berkay Celik, and Ananthram Swami. Practical black-box attacks against machine learning. In *Proceedings of the 2017 ACM on Asia conference on computer and communications security*, pages 506–519, 2017.
- [60] Adnan Siraj Rakin, Jinfeng Yi, Boqing Gong, and Deliang Fan. Defend deep neural networks against adversarial examples via fixed and dynamic quantized activation functions. *arXiv preprint arXiv:1807.06714*, 2018.
- [61] Leslie Rice, Eric Wong, and Zico Kolter. Overfitting in adversarially robust deep learning. In *International Conference on Machine Learning*, pages 8093–8104. PMLR, 2020.
- [62] Adriana Romero, Nicolas Ballas, Samira Ebrahimi Kahou, Antoine Chassang, Carlo Gatta, and Yoshua Bengio. Fitnets: Hints for thin deep nets. *arXiv preprint arXiv:1412.6550*, 2014.

- [63] Andrew Ross and Finale Doshi-Velez. Improving the adversarial robustness and interpretability of deep neural networks by regularizing their input gradients. In *Proceedings of the AAAI Conference on Artificial Intelligence*, 2018.
- [64] Hadi Salman, Andrew Ilyas, Logan Engstrom, Ashish Kapoor, and Aleksander Madry. Do adversarially robust imagenet models transfer better? *arXiv preprint arXiv:2007.08489*, 2020.
- [65] Ludwig Schmidt, Shibani Santurkar, Dimitris Tsipras, Kunal Talwar, and Aleksander Madry. Adversarially robust generalization requires more data. *arXiv preprint arXiv:1804.11285*, 2018.
- [66] Vikash Sehwal, Shiqi Wang, Prateek Mittal, and Suman Jana. Hydra: Pruning adversarially robust neural networks. *Advances in Neural Information Processing Systems (NeurIPS)*, 7, 2020.
- [67] Ali Shafahi, Mahyar Najibi, Amin Ghiasi, Zheng Xu, John Dickerson, Christoph Studer, Larry S Davis, Gavin Taylor, and Tom Goldstein. Adversarial training for free! *arXiv preprint arXiv:1904.12843*, 2019.
- [68] Ali Shafahi, Parsa Saadatpanah, Chen Zhu, Amin Ghiasi, Christoph Studer, David Jacobs, and Tom Goldstein. Adversarially robust transfer learning. In *International Conference on Learning Representations*, 2019.
- [69] Zhiqiang Shen, Zhankui He, and Xiangyang Xue. Meal: Multi-model ensemble via adversarial learning. In *Proceedings of the AAAI Conference on Artificial Intelligence*, volume 33, pages 4886–4893, 2019.
- [70] Mayank Singh, Abhishek Sinha, Nupur Kumari, Harshitha Machiraju, Balaji Krishnamurthy, and Vineeth N Balasubramanian. Harnessing the vulnerability of latent layers in adversarially trained models. *arXiv preprint arXiv:1905.05186*, 2019.
- [71] Suraj Srinivas and François Fleuret. Knowledge transfer with jacobian matching. In *International Conference on Machine Learning*, pages 4723–4731. PMLR, 2018.
- [72] Christian Szegedy, Wojciech Zaremba, Ilya Sutskever, Joan Bruna, Dumitru Erhan, Ian Goodfellow, and Rob Fergus. Intriguing properties of neural networks. *arXiv preprint arXiv:1312.6199*, 2013.
- [73] Yonglong Tian, Dilip Krishnan, and Phillip Isola. Contrastive representation distillation. In *International Conference on Learning Representations*, 2019.
- [74] Florian Tramèr, Alexey Kurakin, Nicolas Papernot, Ian Goodfellow, Dan Boneh, and Patrick McDaniel. Ensemble adversarial training: Attacks and defenses. *arXiv preprint arXiv:1705.07204*, 2017.
- [75] Dimitris Tsipras, Shibani Santurkar, Logan Engstrom, Alexander Turner, and Aleksander Madry. Robustness may be at odds with accuracy. *arXiv preprint arXiv:1805.12152*, 2018.
- [76] Frederick Tung and Greg Mori. Similarity-preserving knowledge distillation. In *Proceedings of the IEEE International Conference on Computer Vision*, pages 1365–1374, 2019.
- [77] Jonathan Uesato, Jean-Baptiste Alayrac, Po-Sen Huang, Robert Stanforth, Alhussein Fawzi, and Pushmeet Kohli. Are labels required for improving adversarial robustness? *arXiv preprint arXiv:1905.13725*, 2019.
- [78] Bao Wang, Alex T Lin, Wei Zhu, Penghang Yin, Andrea L Bertozzi, and Stanley J Osher. Adversarial defense via data dependent activation function and total variation minimization. *arXiv preprint arXiv:1809.08516*, 2018.
- [79] Yisen Wang, Difan Zou, Jinfeng Yi, James Bailey, Xingjun Ma, and Quanquan Gu. Improving adversarial robustness requires revisiting misclassified examples. In *International Conference on Learning Representations*, 2019.
- [80] Eric Wong, Leslie Rice, and J Zico Kolter. Fast is better than free: Revisiting adversarial training. *arXiv preprint arXiv:2001.03994*, 2020.
- [81] Boxi Wu, Jinghui Chen, Deng Cai, Xiaofei He, and Quanquan Gu. Does network width really help adversarial robustness? *arXiv preprint arXiv:2010.01279*, 2020.
- [82] Dongxian Wu, Shu-Tao Xia, and Yisen Wang. Adversarial weight perturbation helps robust generalization. *Advances in Neural Information Processing Systems*, 33, 2020.
- [83] Chang Xiao, Peilin Zhong, and Changxi Zheng. Resisting adversarial attacks by k-winners-take-all. *arXiv preprint arXiv:1905.10510*, 1(2), 2019.
- [84] Cihang Xie and Alan Yuille. Intriguing properties of adversarial training at scale. In *ICLR*, 2020.

- [85] Cihang Xie, Yuxin Wu, Laurens van der Maaten, Alan L Yuille, and Kaiming He. Feature denoising for improving adversarial robustness. In *Proceedings of the IEEE/CVF Conference on Computer Vision and Pattern Recognition*, pages 501–509, 2019.
- [86] Cihang Xie, Mingxing Tan, Boqing Gong, Alan Yuille, and Quoc V Le. Smooth adversarial training. *arXiv preprint arXiv:2006.14536*, 2020.
- [87] Kaidi Xu, Sijia Liu, Gaoyuan Zhang, Mengshu Sun, Pu Zhao, Quanfu Fan, Chuang Gan, and Xue Lin. Interpreting adversarial examples by activation promotion and suppression. *arXiv preprint arXiv:1904.02057*, 2019.
- [88] Shaokai Ye, Kaidi Xu, Sijia Liu, Hao Cheng, Jan-Henrik Lambrechts, Huan Zhang, Aojun Zhou, Kaisheng Ma, Yanzhi Wang, and Xue Lin. Adversarial robustness vs. model compression, or both? In *Proceedings of the IEEE/CVF International Conference on Computer Vision*, pages 111–120, 2019.
- [89] Junho Yim, Donggyu Joo, Jihoon Bae, and Junmo Kim. A gift from knowledge distillation: Fast optimization, network minimization and transfer learning. In *Proceedings of the IEEE Conference on Computer Vision and Pattern Recognition*, pages 4133–4141, 2017.
- [90] Sergey Zagoruyko and Nikos Komodakis. Paying more attention to attention: Improving the performance of convolutional neural networks via attention transfer. *arXiv preprint arXiv:1612.03928*, 2016.
- [91] Sergey Zagoruyko and Nikos Komodakis. Wide residual networks. *NIN*, 8:35–67, 2016.
- [92] Runtian Zhai, Tianle Cai, Di He, Chen Dan, Kun He, John Hopcroft, and Liwei Wang. Adversarially robust generalization just requires more unlabeled data. *arXiv preprint arXiv:1906.00555*, 2019.
- [93] Chiyuan Zhang, Samy Bengio, Moritz Hardt, Benjamin Recht, and Oriol Vinyals. Understanding deep learning requires rethinking generalization. *arXiv preprint arXiv:1611.03530*, 2016.
- [94] Dinghuai Zhang, Tianyuan Zhang, Yiping Lu, Zhanxing Zhu, and Bin Dong. You only propagate once: Accelerating adversarial training via maximal principle. *arXiv preprint arXiv:1905.00877*, 2019.
- [95] Hongyang Zhang, Yaodong Yu, Jiantao Jiao, Eric Xing, Laurent El Ghaoui, and Michael Jordan. Theoretically principled trade-off between robustness and accuracy. In *International Conference on Machine Learning*, pages 7472–7482. PMLR, 2019.
- [96] Hongyi Zhang, Moustapha Cisse, Yann N Dauphin, and David Lopez-Paz. mixup: Beyond empirical risk minimization. *arXiv preprint arXiv:1710.09412*, 2017.
- [97] Jingfeng Zhang, Xilie Xu, Bo Han, Gang Niu, Lizhen Cui, Masashi Sugiyama, and Mohan Kankanhalli. Attacks which do not kill training make adversarial learning stronger. In *International Conference on Machine Learning*, pages 11278–11287. PMLR, 2020.
- [98] Jingfeng Zhang, Jianing Zhu, Gang Niu, Bo Han, Masashi Sugiyama, and Mohan Kankanhalli. Geometry-aware instance-reweighted adversarial training. *arXiv preprint arXiv:2010.01736*, 2020.
- [99] Linjun Zhang, Zhun Deng, Kenji Kawaguchi, Amirata Ghorbani, and James Zou. How does mixup help with robustness and generalization? *arXiv preprint arXiv:2010.04819*, 2020.
- [100] Tianyuan Zhang and Zhanxing Zhu. Interpreting adversarially trained convolutional neural networks. In *International Conference on Machine Learning*, pages 7502–7511. PMLR, 2019.
- [101] Yao Zhu, Jiacheng Ma, Jiacheng Sun, Zewei Chen, Rongxin Jiang, Yaowu Chen, and Zhenguo Li. Towards understanding the generative capability of adversarially robust classifiers. In *Proceedings of the IEEE/CVF International Conference on Computer Vision*, pages 7728–7737, 2021.

Supplementary Material

A Experimental Results

A.1 Additional Details of Experimental Setup

Baselines: For fair comparisons with other methods, we either use the best results reported in the paper or retrained models with optimal hyper-parameters described by the papers. Details of comparison for all the experimental results in the main text are as follows. For Table 1, we take clean accuracy and auto-attack results from [18] and PGD-100 results are the best PGD attack reported results (with the same or similar setting as ours) taken from the respective papers. For Table 2, we take Shafahi et al. [67], Wong et al. [80]’s reported results and evaluated our model with the same settings of PGD attack. For Table 3, we train the same models with PGD7-AT [50], RKD [26] and our method. For PGD7-AT and RKD, we use optimal hyper-parameters reported in the papers. For Table 4, we train the same models with PGD7-AT [50], and our method and evaluated all models with the same settings of PGD attack. The size ratio is computed based on the number of trainable parameters of the student to the trainable parameters of teacher. The purpose of Table 5 is a comparison of our method with IGAM [16] under transfer learning settings. We used PGD7-AT and normal results reported by them. Unlike them, however, results of our method are mean of five repetitions. For Figure 3, we train the same models with the same proportion of data with PGD7-AT and our method.

Adversarial Training: We use standard PGD-7 Adversarial Training with the step size of $2/255$ and $\epsilon = 8/255$.

Teacher Models: We use four teachers in the paper. For most of our CIFAR experiments, we use a WideResNet-28-10 trained by Gowal et al. [29]. For some experiments, we also use WideResNet-34-20 trained on CIFAR-10 by Gowal et al. [29] and WideResNet-28-10 trained on tiny ImageNet trained by [33]. For ImageNet experiments, we use ResNet-50 provided by [64].

Student Models: Student models share all the architectural design of respective teachers e.g. if teacher model by Gowal et al. [29] uses Swish activation function, student models also uses Swish activation. For main CIFAR-10 experiments, we use WideResNet-34-10 following many relevant works like Zhang et al. [95], Chan et al. [16], Pang et al. [56], etc. We also use students with different widths (20, 10, 5, 1) and depths (34, 28, 22, 16, 10). For ImageNet, we use ResNet50 following [67, 80].

Optimizer Setting: For CIFAR experiments, we use SGD with Nesterov momentum 0.9, initial learning rate of 0.1, cosine annealing learning rate decay without restarts, weight decay of 5×10^{-4} and a batch size of 128. For ImageNet, the model is trained for 120 epochs by SGD with a momentum 0.9, weight decay of 5×10^{-5} , batch size of 2048, initial learning rate of 0.8, and cosine learning rate decay. We also use a gradual warmup strategy that increases the learning rate from 0.16 to 0.8 linearly in the first 5 epochs.

Augmentation: All the experiments of our method use Mixup augmentation with coefficient 1 for CIFAR and 0.2 for ImageNet; unless mentioned otherwise. For CIFAR, we also use standard augmentation: randomly cropping a part of 32×32 from the padded image followed by a random horizontal flip provided by PyTorch. For ImageNet, we do two experiments: one with only mixup and one with mixup and random augmentation.

Hyper-parameter Selection: Our method adds a new hyper-parameter α_{acm} . Two other hyper-parameters of our loss are α_{kld} and temperature γ . The selection process for them is detailed in Section A.4. For α_{acm} , we use ablation study to find optimal range of α_{acm} and all of the other experiments are done with $\alpha_{acm} \in \{2000, 5000\}$ and best results are reported.

Compute Infrastructure: We train CIFAR models on one NVIDIA Tesla V100. For ImageNet, we train models in a distributed fashion using 32 GPUs in the cloud.

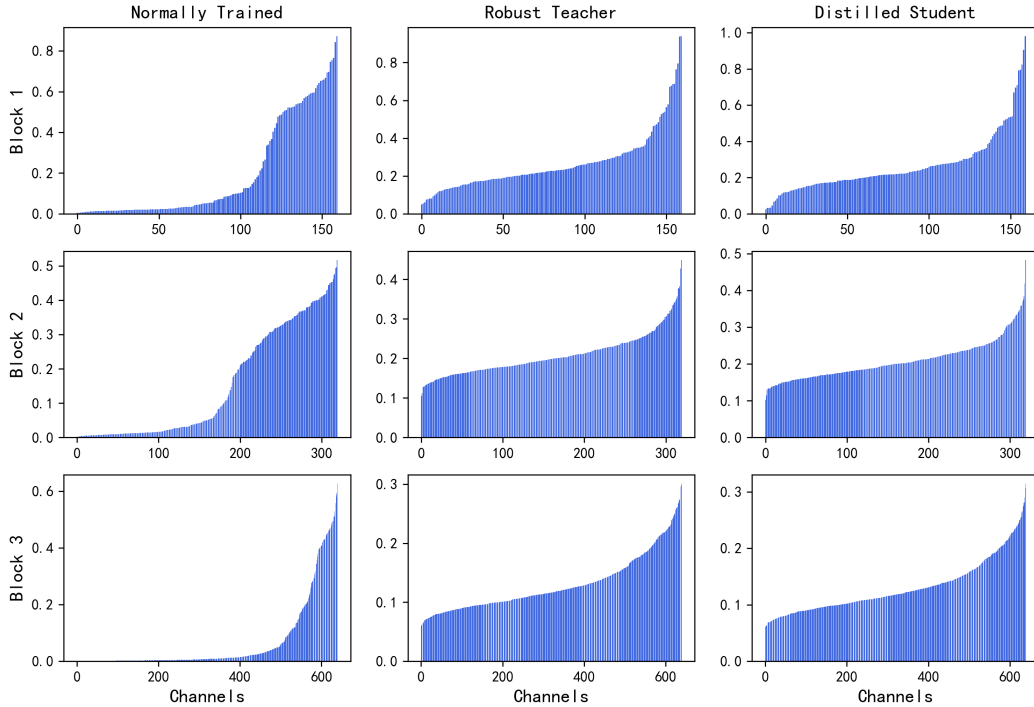


Figure 5: **Comparison of Activated Channel Maps.** Comparison of Activated Channel Maps of a normally trained model, robust teacher and student trained with the proposed method. The x -axis of figure represents channel number of a specific layer and y -axis represents ACM value. Our method makes ACM of student similar to the robust teacher.

A.2 Activated Channel Maps

Our method transfers robustness by matching Activated Channel Maps (ACMs) of robust teacher and student on natural examples. To get Activated Channel Maps, we first get an output of a model at a specific layer called activations \mathcal{A} . These activations are then passed through a mapping function to get activation maps: $a_i = g_c(\mathcal{A}_i)$ and normalized with the magnitude. This process is illustrated in Figure 4. The size of activated channel map is equal to number of channels in a layer e.g. if activation has a size of $\mathcal{A}_i \in \mathbb{R}^{C \times H \times W}$ then activated channel maps shape will be $a_i \in \mathbb{R}^{C \times 1 \times 1}$.

We show Activated Channel Maps of three different blocks of a normally trained WideResNet-16-10, a robust teacher WideResNet-28-10 and a student WideResNet-16-10 trained with our method in Figure 5. The maps are generated on 500 natural examples of CIFAR-10 test set. The Figure shows an average of maps produced on all the examples and sorted in ascending order. The x -axis in the Figure represents channels and the y -axis represents the Activated Channel Map values. The distribution of Activated Channel Maps of our method is spectacularly similar to the robust teacher.

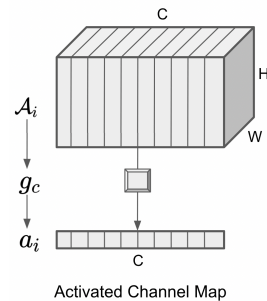
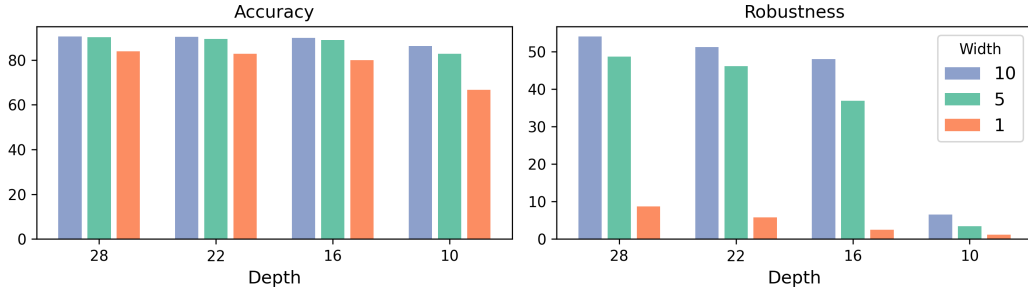


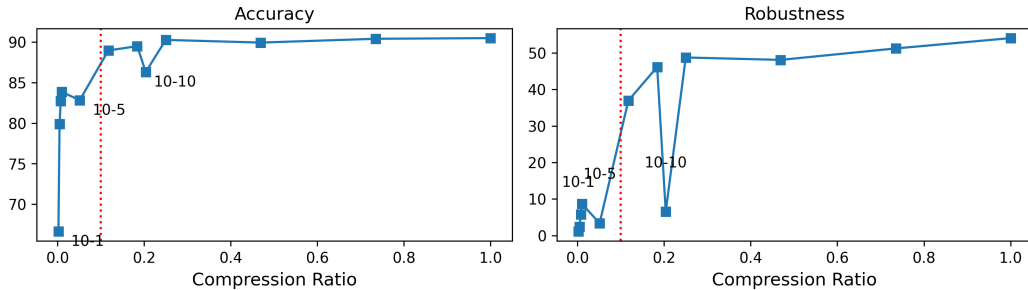
Figure 4: Mapping function g_c is applied channel-wise to get the Activated Channel Maps (ACM).

A.3 Limitation of Proposed Method for Distillation

We show results for distillation with different settings in the paper. To see the limits of our distillation method, we perform an experiment where we progressively reduce the number of channels and layers of the student. The results are shown in Figure 6. For individual values and comparison with PGD7-AT, please see Table 11.



a The figure shows effect of decreasing number of layers and number of channels on accuracy and robustness for our method. The teacher model is a robust WideResNet-28-10 and student models are WideResNet-Depth-Width.



b The figure shows compression ratio vs accuracy and robustness for our method. The dotted red line represents compression ratio of 0.1. Our method works in transferring robustness beyond this point except for dips caused by WideResNet of depth 10.

Figure 6: **Limits of Distillation.** Plots show limits of our method in distilling a large teacher model’s robustness to a small student model without adversarial training.

We observe that our method works well for a compression ratio of > 0.1 (student has $0.1 \times$ teacher’s trainable parameters). We also observe that robustness transfer deteriorates significantly if depth or width is reduced significantly (e.g., depth reduced from 28 to 10; width reduced from 10 to 1). The degradation based on width can be attributed to the transformation function and we expect that other functions may work better. The depth degradation may be due to the representational capability of the student model. We leave further investigation of this for future work.

A.4 Ablation Studies

A.4.1 Effect of Individual Components

To see the effect of individual components of our proposed method, we perform an experiment where we switch different components. The results are shown in Table 7.

In summary, ACM loss alone can transfer significant robustness from the teacher; the addition of soft labels and mixup further improves this transfer. Specifically, robustness with only ACM loss is 48.38%, the addition of soft-labels improves it to 49.53%, the addition of mixup improves it to 52.29%, and the addition of both of these components make final robustness to 56.65%. Also, note that only soft labels are not enough to transfer robustness in this case, as shown by KD Only column. This is in line with the observations of Goldblum et al. [26].

A.4.2 Role of Intermediate Features

To understand the role of low, mid, and high-level features, we performed experiments on CIFAR-10 by progressively changing blocks used for distillation. For this ablation study, we kept all the standard settings reported in the Section A.1. Our correspondence of blocks and features is as follows: block 2: low-level features; block 3: mid-level features; block 4: high-level features. Please note that block 1

Table 7: **Impact of Individual Components.** Impact of different components of our proposed distillation method. We use WideResNet-34-10 as student following Table 1 in the main text.

	Std. Setting	w/o KD	w/o Mixup	Only ACM	Only KD
Mapping Function (g_c)	✓	✓	✓	✓	
Teacher Soft Labels	✓		✓		✓
Mixup	✓	✓			
ACM Loss	✓	✓	✓	✓	
Accuracy	90.76	92.50	91.17	92.87	89.38
Robustness	56.65	52.29	49.53	48.38	0.21

Features Used	Accuracy	Robustness
Low-Level (2)	86.36	17.24
Mid-Level (3)	88.30	39.37
High-Level (4)	91.18	33.13
Low+Mid Level (2+3)	88.15	41.92
Mid+High Level (3+4)	90.69	52.79
First Layer Only (1)	86.00	0.31
No First Layer (2+3+4)	90.69	56.15
All Features	90.76	56.65

Table 8: Impact of using different intermediate features on clean accuracy and robustness of student.

corresponds to the output of the first layer only. Therefore, we do not call it low-level features. The results are shown in the Table 8.

As shown in the Table 8, mid-level features play a more important role in robustness transfer and high-level features play a crucial role in accuracy transfer. The robustness of the student is 39.37% when we only use mid-level features, but it decreases to 33.13% when high-level features are utilized alone. On the other hand, clean accuracy improves when we only use high-level features: 88.30% with mid-level compared with 91.18% with high-level features. In addition, a combination of mid and high-level features is enough to get close to optimal robustness and accuracy. But the addition of low-level features improves robustness even further.

Apart from these low, mid, and high-level features, we also used the output of the first layer in the proposed loss function. Our experiments above show that the improvement brought by first layer distillation is relatively small. Specifically, the addition of the first layer in the above-mentioned experiments brings $\leq 1\%$ improvement for robustness.

In summary, all level features (low, mid, high level) improve robustness and accuracy. However, mid-level features seem to be more critical for robustness and high-level features for accuracy.

A.4.3 Comparison of Losses

The purpose of ACM loss is to match activated channel maps of teacher and student. It is possible to distill robustness by directly matching intermediate features of teacher and student. However, this direct way of distillation overlooks differences between the teacher and the student such as structure, number of channels, size of activations, how and on what data teacher is trained, etc.

To see the effect of directly distilling the intermediate features, we also have conducted an ablation study comparing direct distillation (ℓ_2 -loss) with ACM-based distillation while progressively increasing differences between the teacher and the student. We have kept all the standard settings (Section A.1) and used similar settings for direct distillation for a fair comparison.

The results are reported in Table 9. When teacher and student are similar, ACM performs slightly better than direct distillation (56.65% vs. 56.12%). However, when the number of channels of teacher and student is different, the performance gap increases (48.75% vs. 44.95%). This gap increases further when both channels and the number of layers are different (47.18% vs. 41.90%). A similar gap is also visible in terms of clean accuracy for all these cases.

To further explore the effect of this difference, we also performed one experiment under transfer learning settings for CIFAR-100 (Table 5 in the paper). Here, the teacher is trained on a different

Method	Teacher	Student	Accuracy	Robustness
Distillation for CIFAR-10				
Full	WRN28-10	WRN34-10	89.98	56.12
MixACM	WRN28-10	WRN34-10	90.76	56.65
Full	WRN28-10	WRN28-5	88.46	44.95
MixACM	WRN28-10	WRN28-5	90.26	48.75
Full	WRN-34-20	WRN16-10	84.27	41.9
MixACM.	WRN-34-20	WRN16-10	86.31	47.18
Transfer Learning for CIFAR-100				
Direct	WRN28-10	WRN34-10	57.86	16.20
ACM	WRN28-10	WRN34-10	65.69	24.14

Table 9: Effect of using direct loss vs. MixACM loss on distillation and transfer learning.

dataset (ImageNet), so the difference between the two models is larger. The performance gap is also wider. ACM outperforms direct distillation significantly (clean accuracy: 65.69% vs. 57.86% and robustness: 24.14% vs. 16.20%).

A.4.4 Effect of α_{acm}

The only extra hyper-parameters introduced by our algorithm is the weight of ACM loss (α_{acm}). To see the effect of α_{acm} , we perform an ablation experiment with WideResNet-34-10 as student. To avoid any confounding effect of other factors, we use only ACM loss in this experiment. The results are shown in Figure 7a.

In summary, the clean accuracy of the model is less sensitive to α_{acm} compared with robustness. For instance when we vary the values of α_{acm} from 100000 to 100, the clean accuracy changes from 94 to 92 while robustness changes from 50 to 30. The value of α_{acm} also acts as a trade-off between clean accuracy and robustness.

A.4.5 Effect of α_{kld} and temperature γ

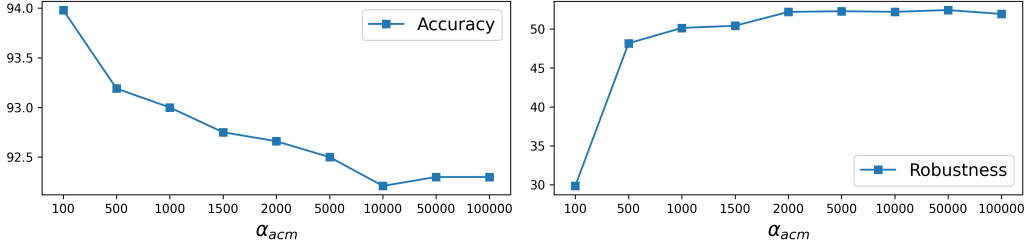
Our proposed method uses soft labels with KLD loss [36]. This loss has two hyper-parameters: α_{kld} and temperature γ . We select best values of these hyper-parameters with an experiment where we set $\alpha_{acm} = 5000$ and tried three different settings of these two parameters. The results are reported in Figure 7b. The student is a WideResNet-34-10. We select best values: $\alpha_{kld} = 0.95, \gamma = 10$. We use these hyper-parameter values for all of our experiments.

A.4.6 Comparison of Transforms

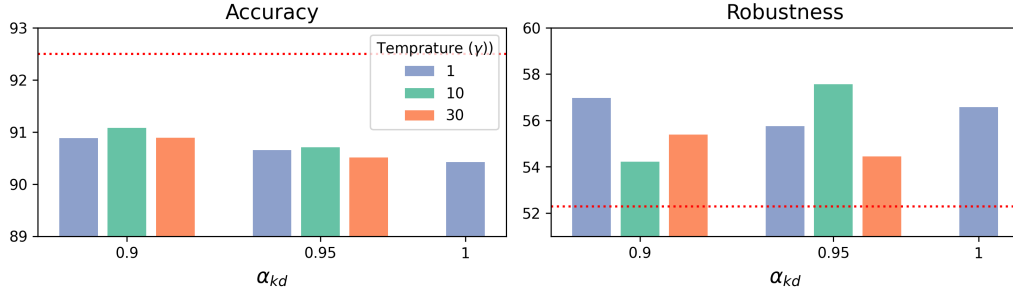
Our method requires a transformation function applied on Activated Channel Maps if teacher and student have different number of channels. For this purpose, we compare performance of three different transformation functions: a fully connected layer, an adaptive average pool function or adaptive max pool function. We applied these functions under two settings: applied on teacher’s activated channel maps or applied on student’s activated channel maps. The results are shown in Table 10.

B Theoretical Results

This appendix has full proofs for results in Section 4. The order is as follows. We first prove that the population adversarial error can be bounded above by the sum of an empirical adversarial loss and a distillation loss. Then we consider a binary classification task with the logistic loss function and prove that the distillation loss can be approximated by the mixup augmentation based loss.



a Effect of α_{acm} on accuracy and robustness.



b Effect of α_{kld} and temperature γ on accuracy and robustness. The dotted red line represents training without soft labels (i.e., $\alpha_{kld} = 0$).

Figure 7: **Hyper-parameter Selection.** Comparison of three different hyper-parameters on accuracy and robustness.

Table 10: Effect of different transformation functions for robustness transfer from robust WideResNet-28-10 to WideResNet-28-5.

Teacher Transform	Student Transform	Accuracy	Robustness
None	Adaptive Max Pool	89.92	46.41
None	Adaptive Avg Pool	90.04	46.27
None	Affine	88.86	30.27
Adaptive Max Pool	None	90.26	48.75
Adaptive Avg Pool	None	89.99	42.01
Affine	None	88.39	23.51

B.1 Proof of Theorem 4.1

Theorem. We consider task of mapping input $x \in \mathcal{X} \subseteq \mathbb{R}^d$ to label $y \in \mathcal{Y} = \{1, 2, \dots, K\}$. Denote the training data as $\mathcal{D} = \{(x_1, y_1), \dots, (x_n, y_n)\}$, where each data point is sampled from a ground truth distribution P . The goal is to learn a classifier $f : \mathcal{X} \rightarrow \mathbb{R}^K$ from a hypothetical space \mathcal{F} . Let $L(f(x), y) = 1 - \phi_\gamma(f(x), y)$ be the loss function, where $\gamma > 0$ is the temperature and

$$\phi_\gamma(f(x), y) = \frac{\exp(f(x)_y/\gamma)}{\sum_{k=1}^K \exp(f(x)_k/\gamma)}.$$

Suppose a classifier f is decomposed into $g \circ h$, where $h \in \mathcal{H}$ is a feature extractor and $g \in \mathcal{G}$ stands for the top model. We considered supervision of a teacher feature extractor $h^T(x)$ trained on same or similar dataset. Then, with probability $1 - \delta$, for any $f \in \mathcal{F}$,

$$\mathbb{E} \left[\max_{\|\delta\|_\infty \leq \epsilon} \mathbb{I}\{\hat{y}(x + \delta) \neq y\} \right] \leq 2\tilde{\mathcal{L}}(f, \mathcal{D}) + \frac{8}{\gamma} \tilde{\mathcal{L}}_{dis}(f, \mathcal{D}) + 4\mathfrak{R}_S(\Psi_T) + \frac{16}{n} + 6\sqrt{\frac{2/\delta}{2n}}, \quad (2)$$

where \mathfrak{R}_S is the Rademacher complexity, $\Psi_T = \{ \max_{\|\delta\|_\infty < \epsilon} L(g \circ h^T(x + \delta), y) : g \in \mathcal{G} \}$ and

$$\tilde{\mathcal{L}}_{dis}(f, \mathcal{D}) = \frac{1}{n} \inf_{g \in \mathcal{G}} \sum_{i=1}^n \max_{\|\delta\|_\infty < \epsilon} |f(x_i + \delta) - g \circ h^T(x_i + \delta)|.$$

Table 11: **Distillation with Different Size Ratios.** The table shows result of distillation from a large teacher to a progressively small student. Size ratio is ratio of number of trainable parameters in student to teacher. Our method works well to reduce teacher size 10 \times . However, significant compression of depth and width causes a sharp deterioration of performance.

Teacher	Student	Size Ratio	PGD7-AT		Ours	
			Acc.	Rob.	Acc.	Rob.
WRN 28-10	WRN 28-10	100%	84.17	49.23	90.48	54.05
	WRN 28-5	25.04%	83.90	47.74	90.26	48.75
	WRN 28-1	1.01%	78.89	48.27	83.86	8.67
	WRN 22-10	73.5%	84.26	49.29	90.40	51.23
	WRN 22-5	18.40%	83.73	48.93	89.49	46.16
	WRN 22-1	0.75%	78.36	47.57	82.74	5.81
WRN 16-10	WRN 16-10	46.92%	83.90	47.55	89.93	48.09
	WRN 16-5	11.76%	83.51	48.11	88.96	36.95
	WRN 16-1	0.48%	75.69	44.46	79.90	2.45
	WRN 10-10	20.38%	78.59	44.41	86.31	6.54
	WRN 10-5	5.12%	78.16	44.04	82.82	3.41
	WRN 10-1	0.21%	67.11	38.85	66.65	1.15

Proof: Denote the adversarial loss with ϵ -bounded ℓ_∞ adversarial attacks as

$$\tilde{L}(f(x), y) = \max_{\|\delta\|_\infty < \epsilon} L(f(x + \delta), y).$$

Let $j \in \{1, \dots, \log_2(n)\}$ and $\tau_j = 2^{2-j}$. Here, for simplicity, we assume $\log_2(n)$ is a positive integer. Then, we denote the following classes of functions $\Psi_T = \{\tilde{L}(g \circ h^T(x), y) : g \in \mathcal{G}\}$ and

$$\Psi_j = \{\tilde{L}(f(x), y) : \inf_{g \in \mathcal{G}} \frac{1}{n} \sum_{i=1}^n |\tilde{L}(f(x_i), y_i) - \tilde{L}(g \circ h^T(x_i), y_i)| \leq \tau_j\}.$$

By the classical generalization bound with the Rademacher complexity, with probability at least $1 - \delta$, for any $\tilde{L} \in \Psi_j$,

$$\mathbb{E}[\tilde{L}(f(x), y)] \leq \frac{1}{n} \sum_{i=1}^n \tilde{L}(f(x_i), y_i) + 2\mathfrak{R}_S(\Psi_j) + 3\sqrt{\frac{2/\delta}{2n}}, \quad (3)$$

where

$$\mathfrak{R}_S(\Psi_j) = \frac{1}{n} \mathbb{E}_\epsilon \left[\sup_{\tilde{L}(f) \in \Psi_j} \sum_{i=1}^n \epsilon_i \tilde{L}(f(x_i), y_i) \right].$$

Furthermore, we have

$$\begin{aligned} \mathfrak{R}_S(\Psi_j) &= \frac{1}{n} \mathbb{E}_\epsilon \left[\sup_{\tilde{L} \in \Psi_j} \inf_{g \in \mathcal{G}} \sum_{i=1}^n \epsilon_i \tilde{L}(f(x_i), y_i) \right] \\ &= \frac{1}{n} \mathbb{E}_\epsilon \left[\sup_{\tilde{L}(f) \in \Psi_j} \inf_{g \in \mathcal{G}} \sum_{i=1}^n \epsilon_i (\tilde{L}(f(x_i), y_i) - \tilde{L}(g \circ h^T(x_i), y_i) + \tilde{L}(g \circ h^T(x_i), y_i)) \right] \\ &\leq \frac{1}{n} \mathbb{E}_\epsilon \left[\sup_{\tilde{L}(f) \in \Psi_j} \inf_{g \in \mathcal{G}} \max_i |\epsilon_i| \sum_{i=1}^n |\tilde{L}(f(x_i), y_i) - \tilde{L}(g \circ h^T(x_i), y_i)| \right] \\ &\quad + \frac{1}{n} \mathbb{E}_\epsilon \left[\sup_{g \in \mathcal{G}} \sum_{i=1}^n \epsilon_i \tilde{L}(g \circ h^T(x_i), y_i) \right] \\ &\leq \tau_j + \mathfrak{R}_S(\Psi_T). \end{aligned}$$

Plugging the upper bound of $\mathfrak{R}_S(\Psi_j)$ into (3), we have with probability at least $1 - \delta$,

$$\mathbb{E}[\tilde{L}(f(x), y)] \leq \frac{1}{n} \sum_{i=1}^n \tilde{L}(f(x_i), y_i) + 2\tau_j + 2\mathfrak{R}_S(\Psi_T) + 3\sqrt{\frac{2/\delta}{2n}}. \quad (4)$$

Then the inequality (4) holds for all $f \in \mathcal{F}$ and j with probability at least $1 - \log_2(n)\delta$. Given f , then for any $g \in \mathcal{G}$,

$$\frac{1}{n} \sum_{i=1}^n |\tilde{L}(f(x_i), y_i) - \tilde{L}(g \circ h^T(x_i), y_i)| \leq 2.$$

This implies that for any given f , there exists $j \in \{1, \dots, \log_2(n)\}$ such that $\tilde{L}(f(x), y) \in \Psi_j$. We select the smallest j that satisfies

$$\tau_j \geq \frac{1}{n} \inf_{g \in \mathcal{G}} \sum_{i=1}^n |\tilde{L}(f(x_i), y_i) - \tilde{L}(g \circ h^T(x_i), y_i)| \geq \frac{1}{2}\tau_j - 2^{1-\log_2(n)}.$$

Then

$$\tau_j \leq \frac{4}{n} + \frac{2}{n} \inf_{g \in \mathcal{G}} \sum_{i=1}^n |\tilde{L}(f(x_i), y_i) - \tilde{L}(g \circ h^T(x_i), y_i)|.$$

Furthermore, the inequality (4) can be rewritten as

$$\begin{aligned} \mathbb{E}[\tilde{L}(f(x), y)] &\leq \frac{1}{n} \sum_{i=1}^n \tilde{L}(f(x_i), y_i) + \frac{8}{n} \\ &\quad + \frac{4}{n} \inf_{g \in \mathcal{G}} \sum_{i=1}^n |\tilde{L}(f(x_i), y_i) - \tilde{L}(g \circ h^T(x_i), y_i)| \\ &\quad + 2\mathfrak{R}_S(\Psi_T) + 3\sqrt{\frac{2/\delta}{2n}}, \end{aligned} \quad (5)$$

with probability at least $1 - \delta$. In addition,

$$\begin{aligned} \tilde{L}(f(x), y) &\leq \max_{\|\delta\|_\infty < \epsilon} |L(f(x), y) - L(g \circ h^T(x), y)| + \tilde{L}(g \circ h^T(x), y), \\ \tilde{L}(g \circ h^T(x), y) &\leq \max_{\|\delta\|_\infty < \epsilon} |L(f(x), y) - L(g \circ h^T(x), y)| + \tilde{L}(f(x), y). \end{aligned}$$

So we have

$$\begin{aligned} \mathbb{E}[\tilde{L}(f(x), y)] &\leq \frac{1}{n} \sum_{i=1}^n \tilde{L}(f(x_i), y_i) + \frac{8}{n} \\ &\quad + \frac{4}{n} \inf_{g \in \mathcal{G}} \sum_{i=1}^n \max_{\|\delta\|_\infty < \epsilon} |L(f(x_i + \delta), y_i) - L(g \circ h^T(x_i + \delta), y_i)| \\ &\quad + 2\mathfrak{R}_S(\Psi_T) + 3\sqrt{\frac{2/\delta}{2n}}, \end{aligned}$$

Next we show the relationship between the adversarial accuracy and $\mathbb{E}[\tilde{L}(f(x), y)]$. The adversarial loss function \tilde{L} can be rewritten as

$$\begin{aligned} \tilde{L}(f(x), y) &= \max_{\|\delta\|_\infty < \epsilon} \frac{\sum_{k \neq y} \exp(f(x + \delta)_k / \gamma)}{\sum_{k \in [K]} \exp(f(x + \delta)_k / \gamma)} \\ &= \max_{\|\delta\|_\infty < \epsilon} \frac{1}{1 + \frac{\exp(f(x + \delta)_y / \gamma)}{\sum_{k \neq y} \exp(f(x + \delta)_k / \gamma)}} \\ &= \max_{\|\delta\|_\infty < \epsilon} \frac{1}{1 + \exp(f(x + \delta)_y / \gamma) - \ln(\sum_{k \neq y} \exp(f(x + \delta)_k / \gamma))} \\ &= \max_{\|\delta\|_\infty < \epsilon} \sigma\left(-\frac{f(x + \delta)_y}{\gamma} + \ln\left(\sum_{k \neq y} \exp\left(\frac{f(x + \delta)_k}{\gamma}\right)\right)\right), \end{aligned} \quad (6)$$

where σ is the sigmoid function. Notice that σ is a monotonically increasing function and

$$\ln \left(\sum_{k \neq y} \exp\left(\frac{f(x + \delta)_k}{\gamma}\right) \right) \geq \max_{k \neq y} \frac{f(x + \delta)_k}{\gamma}.$$

Then we have

$$\tilde{L}(f(x), y) \geq \max_{\|\delta\|_\infty < \epsilon} \sigma \left(-\frac{f(x + \delta)_y}{\gamma} + \max_{k \neq y} \frac{f(x + \delta)_k}{\gamma} \right) \quad (7)$$

If there exists δ such that $f(x + \delta)_y \leq \max_{k \neq y} f(x + \delta)_k$, then

$$\max_{\|\delta\|_\infty < \epsilon} \sigma \left(-\frac{f(x + \delta)_y}{\gamma} + \max_{k \neq y} \frac{f(x + \delta)_k}{\gamma} \right) \geq \frac{1}{2} \max_{\|\delta\|_\infty < \epsilon} \mathbb{I}(f(x + \delta)_y \leq \max_{k \neq y} f(x + \delta)_k). \quad (8)$$

In contrast, if for any δ , $f(x + \delta)_y > \max_{k \neq y} f(x + \delta)_k$, then

$$\sigma \left(-\frac{f(x + \delta)_y}{\gamma} + \max_{k \neq y} \frac{f(x + \delta)_k}{\gamma} \right) \geq \mathbb{I}(f(x + \delta)_y \leq \max_{k \neq y} f(x + \delta)_k). \quad (9)$$

Combining (8) and (9),

$$2\tilde{L}(f(x), y) \geq \max_{\|\delta\|_\infty < \epsilon} \mathbb{I}(f(x + \delta)_y \leq \max_{k \neq y} f(x + \delta)_k). \quad (10)$$

According to (5) and (10), we have

$$\begin{aligned} & \mathbb{P}[\{(x, y) : \exists \delta, \|\delta\|_\infty < \epsilon \text{ s.t. } \hat{y}(x + \delta) \neq y\}] \\ &= \mathbb{E} \left[\max_{\|\delta\|_\infty < \epsilon} \mathbb{I}(f(x + \delta)_y \leq \max_{k \neq y} f(x + \delta)_k) \right] \\ &\leq 2\mathbb{E}[\tilde{L}(f(x), y)] \\ &\leq \frac{2}{n} \sum_{i=1}^n \tilde{L}(f(x_i), y_i) + \frac{16}{n} \\ &\quad + \frac{8}{n} \inf_{g \in \mathcal{G}} \sum_{i=1}^n \max_{\|\delta\|_\infty < \epsilon} |L(f(x_i + \delta), y_i) - L(g \circ h^T(x_i + \delta), y_i)| \\ &\quad + 4\mathfrak{R}_S(\Psi_T) + 6\sqrt{\frac{2/\delta}{2n}}, \end{aligned}$$

with probability at least $1 - \delta$. According to [25],

$$\begin{aligned} & \mathbb{P}[\{(x, y) : \exists \delta, \|\delta\|_\infty < \epsilon \text{ s.t. } \hat{y}(x + \delta) \neq y\}] \\ &\leq \frac{2}{n} \sum_{i=1}^n \tilde{L}(f(x_i), y_i) + \frac{16}{n} \\ &\quad + \frac{8}{n\gamma} \inf_{g \in \mathcal{G}} \sum_{i=1}^n \max_{\|\delta\|_\infty < \epsilon} |f(x_i + \delta) - g \circ h^T(x_i + \delta)| \\ &\quad + 4\mathfrak{R}_S(\Psi_T) + 6\sqrt{\frac{2/\delta}{2n}}. \end{aligned}$$

□

B.2 Proof of Theorem 4.2

In this section, we start with a binary classification task and logistic regression. Denote

$$f_\theta(x) = \theta^\top x, \quad g(f_\theta(x)) = \frac{1}{1 + \exp(-f_\theta(x))}, \quad h(f_\theta(x)) = \log(1 + \exp(f_\theta(x))).$$

Then the loss function L can be rewritten as

$$L(f_\theta(x), y) = h(f_\theta(x)) - yf_\theta(x).$$

Notice that $\|\delta\|_\infty \leq \epsilon$ implies $\|\delta\|_2 \leq \epsilon\sqrt{d}$, and therefore

$$\max_{\|\delta\|_\infty \leq \epsilon} L(f_\theta(x), y) \leq \max_{\|\delta\|_2 \leq \epsilon\sqrt{d}} L(f_\theta(x), y),$$

where d is the dimension of the input x . The standard empirical loss function can be written as

$$\mathcal{L}(f_\theta, \mathcal{D}) = \frac{1}{n} \sum_{i=1}^n L(f_\theta(\mathbf{x}_i), \mathbf{y}_i) = \frac{1}{n} \sum_{i=1}^n h(f_\theta(\mathbf{x}_i)) - \mathbf{y}_i f_\theta(\mathbf{x}_i),$$

where $\mathcal{D} = \{(\mathbf{x}_i, \mathbf{y}_i), i = 1, \dots, n\}$. For a given $\epsilon > 0$, we consider the adversarial loss with l_2 -attack of size $\epsilon\sqrt{d}$, that is,

$$\tilde{\mathcal{L}}(f_\theta, \mathcal{D}) = \frac{1}{n} \sum_{i=1}^n \max_{\|\delta_i\|_2 \leq \epsilon\sqrt{d}} \tilde{L}(f_\theta(\mathbf{x}_i + \delta_i), \mathbf{y}_i) = \frac{1}{n} \sum_{i=1}^n \tilde{L}(f_\theta(\mathbf{x}_i), \mathbf{y}_i)$$

Consider the data-dependent parameter space:

$$\Theta = \{ \theta \in \mathbb{R}^d : \mathbf{y}_i f_\theta(\mathbf{x}_i) + (\mathbf{y}_i - 1) f_\theta(\mathbf{x}_i) \geq 0, \\ \text{and } |\mathbf{y}_i^* - g(f_\theta(\mathbf{x}_i))| \leq \beta |\mathbf{y}_i - g(f_\theta(\mathbf{x}_i))|, \text{ for all } i = 1, \dots, n \}.$$

The first inequality considers the zero training error (0-1 loss). That is $f_\theta(\mathbf{x}) > 0$ when $\mathbf{y} = 1$ and $f_\theta(\mathbf{x}) \leq 0$ if $\mathbf{y} = 0$. The second inequality constraints the distillation, i.e. $g(f_\theta(\mathbf{x}_i))$ is closed to the soft label given by the teacher model. Now we are ready to state the following theorem:

Theorem. *Suppose there exists a constant $c_x > 0$ such that $\|\mathbf{x}_i\|_2 > c_x\sqrt{d}$ for all $i \in \{1, \dots, n\}$. Then, for any $\theta \in \Theta$, we have*

$$\tilde{\mathcal{L}}(f_\theta, \mathcal{D}) + \alpha \tilde{\mathcal{L}}(f_\theta, \mathcal{D}_{dis}) \leq \mathcal{L}_{mix}(f_\theta, \mathcal{D}) + \alpha \mathcal{L}_{mix}(f_\theta, \mathcal{D}_{dis}),$$

where the size of the adversarial attack ϵ is

$$\epsilon = \frac{1 - \alpha\beta}{1 + \beta} c_x R \mathbb{E}_{\lambda \sim \tilde{P}_\lambda} [1 - \lambda], \quad \text{with } R = \min_{i \in \{1, \dots, n\}} |\cos(\theta, \mathbf{x}_i)|,$$

and the distribution \tilde{P}_λ is

$$\tilde{P}_\lambda(\lambda) = \frac{\alpha}{\alpha + \beta} \text{Beta}(\alpha + 1, \beta) + \frac{\beta}{\alpha + \beta} \text{Beta}(\beta + 1, \alpha).$$

Proof: By the second order Taylor approximation,

$$L(f_\theta(x + \delta), y) \approx L(f_\theta(x), y) + \delta^\top \frac{\partial}{\partial x} L(f_\theta(x), y) + \frac{1}{2} \delta^\top \frac{\partial^2}{\partial x \partial x^\top} L(f_\theta(x), y) \delta.$$

Note that

$$\begin{aligned} \frac{\partial}{\partial x} L(f_\theta(x), y) &= \frac{\partial}{\partial x} (h(f_\theta(x)) - y f_\theta(x)) \\ &= \frac{\partial}{\partial f} h(f_\theta(x)) \frac{\partial}{\partial x} f_\theta(x) - y \frac{\partial}{\partial x} f_\theta(x) \\ &= g(f_\theta(x)) \theta - y \theta \\ &= (g(\theta^\top x) - y) \theta \end{aligned}$$

and

$$\begin{aligned} \frac{\partial^2}{\partial x \partial x^\top} L(f_\theta(x), y) &= \frac{\partial^2}{\partial x \partial x^\top} (h(f_\theta(x)) - y f_\theta(x)) \\ &= \frac{\partial^2}{\partial f \partial f} h(f_\theta(x)) \left(\frac{\partial}{\partial x} f_\theta(x) \right)^2 \\ &= \frac{\partial}{\partial f} g(f_\theta(x)) \theta \theta^\top \\ &= g(\theta^\top x) (1 - g(\theta^\top x)) \theta \theta^\top. \end{aligned}$$

So we have

$$L(f_\theta(x + \delta), y) \approx L(f_\theta(x), y) + (g(\theta^\top x) - y)\theta^\top \delta + \frac{1}{2}g(\theta^\top x)(1 - g(\theta^\top x))(\theta^\top \delta)^2$$

Furthermore

$$\begin{aligned} \tilde{\mathcal{L}}(f_\theta, \mathcal{D}) &\approx \frac{1}{n} \sum_{i=1}^n L(f_\theta(\mathbf{x}_i), \mathbf{y}_i) + \frac{1}{n} \sum_{i=1}^n \max_{\|\delta_i\|_2 \leq \epsilon\sqrt{d}} \left\{ (g(\theta^\top \mathbf{x}_i) - \mathbf{y}_i)\theta^\top \delta_i \right. \\ &\quad \left. + \frac{1}{2}g(\theta^\top \mathbf{x}_i)(1 - g(\theta^\top \mathbf{x}_i))(\theta^\top \delta_i)^2 \right\} \\ &=: \frac{1}{n} \sum_{i=1}^n L(f_\theta(\mathbf{x}_i), \mathbf{y}_i) + I_1. \end{aligned}$$

Similarly, for the data $\mathcal{D}_{dis} = \{(\mathbf{x}_i, \mathbf{y}_i^*), \mathbf{y}_i^* = f^T(\mathbf{x}_i), i = 1, \dots, n\}$,

$$\begin{aligned} \tilde{\mathcal{L}}(f_\theta, \mathcal{D}_{dis}) &\approx \frac{1}{n} \sum_{i=1}^n L(f_\theta(\mathbf{x}_i), \mathbf{y}_i^*) + \frac{1}{n} \sum_{i=1}^n \max_{\|\delta_i\|_2 \leq \epsilon\sqrt{d}} \left\{ (g(\theta^\top \mathbf{x}_i) - \mathbf{y}_i^*)\theta^\top \delta_i \right. \\ &\quad \left. + \frac{1}{2}g(\theta^\top \mathbf{x}_i)(1 - g(\theta^\top \mathbf{x}_i))(\theta^\top \delta_i)^2 \right\} \\ &=: \frac{1}{n} \sum_{i=1}^n L(f_\theta(\mathbf{x}_i), \mathbf{y}_i^*) + I_2. \end{aligned}$$

Therefore,

$$\tilde{\mathcal{L}}(f_\theta, \mathcal{D}) + \alpha \tilde{\mathcal{L}}(f_\theta, \mathcal{D}_{dis}) = \frac{1}{n} \sum_{i=1}^n L(f_\theta(\mathbf{x}_i), \mathbf{y}_i) + \frac{\alpha}{n} \sum_{i=1}^n L(f_\theta(\mathbf{x}_i), \mathbf{y}_i^*) + I_1 + \alpha I_2.$$

Furthermore

$$\begin{aligned} I_1 + \alpha I_2 &\leq \frac{1}{n} \sum_{i=1}^n \max_{\|\delta_i\|_2 \leq \epsilon\sqrt{d}} \left((g(\theta^\top \mathbf{x}_i) - \mathbf{y}_i)\theta^\top \delta_i \right) \\ &\quad + \frac{\alpha}{n} \sum_{i=1}^n \max_{\|\delta_i\|_2 \leq \epsilon\sqrt{d}} \left((g(\theta^\top \mathbf{x}_i) - \mathbf{y}_i^*)\theta^\top \delta_i \right) \\ &\quad + (1 + \alpha) \frac{1}{2n} \sum_{i=1}^n \max_{\|\delta_i\|_2 \leq \epsilon\sqrt{d}} g(\theta^\top \mathbf{x}_i)(1 - g(\theta^\top \mathbf{x}_i))(\theta^\top \delta_i)^2 \\ &= \frac{\epsilon\sqrt{d}}{n} \sum_{i=1}^n |g(\theta^\top \mathbf{x}_i) - \mathbf{y}_i| \|\theta\|_2 + \frac{\alpha\epsilon\sqrt{d}}{n} \sum_{i=1}^n |g(\theta^\top \mathbf{x}_i) - \mathbf{y}_i^*| \|\theta\|_2 \\ &\quad + (1 + \alpha)\epsilon^2 d \frac{1}{2n} \sum_{i=1}^n g(\theta^\top \mathbf{x}_i)(1 - g(\theta^\top \mathbf{x}_i)) \|\theta\|_2^2. \end{aligned}$$

Next we shall bound $\tilde{\mathcal{L}}(f_\theta, \mathcal{D}) + \alpha \tilde{\mathcal{L}}(f_\theta, \mathcal{D}_{dis})$ by mixup augmentation. Consider the following loss:

$$\begin{aligned} \mathcal{L}_{mix}(f_\theta, \mathcal{D}) &= \frac{1}{n^2} \sum_{i=1}^n \sum_{j=1}^n \mathbb{E}_{\lambda \sim P_\lambda} [L(f_\theta(\mathbf{x}_{ij}(\lambda)), \mathbf{y}_{ij}(\lambda))], \\ \mathcal{L}_{mix}(f_\theta, \mathcal{D}_{dis}) &= \frac{1}{n^2} \sum_{i=1}^n \sum_{j=1}^n \mathbb{E}_{\lambda \sim P_\lambda} [L(f_\theta(\mathbf{x}_{ij}(\lambda)), \mathbf{y}_{ij}^*(\lambda))], \end{aligned}$$

where P_λ is a Beta distribution $\text{Beta}(\alpha, \beta)$, $\mathbf{y}_{ij}(\lambda) = \lambda \mathbf{y}_i + (1-\lambda)\mathbf{y}_j$ and $\mathbf{y}_{ij}^*(\lambda) = \lambda \mathbf{y}_i^* + (1-\lambda)\mathbf{y}_j^*$. We start with $\mathcal{L}_{mix}(f_\theta, \mathcal{D})$:

$$\begin{aligned}\mathcal{L}_{mix}(f_\theta, \mathcal{D}) &= \frac{1}{n^2} \sum_{i=1}^n \sum_{j=1}^n \mathbb{E}_{\lambda \sim P_\lambda} [h(\theta^\top \mathbf{x}_{ij}(\lambda)) - \mathbf{y}_{ij}(\lambda) \theta^\top \mathbf{x}_{ij}(\lambda)] \\ &= \frac{1}{n^2} \sum_{i=1}^n \sum_{j=1}^n \mathbb{E}_{\lambda \sim P_\lambda} \left\{ \lambda [h(\theta^\top \mathbf{x}_{ij}(\lambda)) - \mathbf{y}_i \theta^\top \mathbf{x}_{ij}(\lambda)] \right. \\ &\quad \left. + (1-\lambda) [h(\theta^\top \mathbf{x}_{ij}(\lambda)) - \mathbf{y}_j \theta^\top \mathbf{x}_{ij}(\lambda)] \right\}\end{aligned}$$

We introduce a 0-1 random variable B such that the conditional distribution of B given λ is

$$P(B = 1|\lambda) = \lambda, \quad \text{and} \quad P(B = 0|\lambda) = 1 - \lambda.$$

Rewrite $\mathcal{L}_{mix}(f_\theta, \mathcal{D})$ as

$$\begin{aligned}\mathcal{L}_{mix}(f_\theta, \mathcal{D}) &= \frac{1}{n^2} \sum_{i=1}^n \sum_{j=1}^n \mathbb{E}_{\lambda \sim P_\lambda} \left\{ \mathbb{E}_{B|\lambda} \left\{ B [h(\theta^\top \mathbf{x}_{ij}(\lambda)) - \mathbf{y}_i \theta^\top \mathbf{x}_{ij}(\lambda)] \right. \right. \\ &\quad \left. \left. + (1-B) [h(\theta^\top \mathbf{x}_{ij}(\lambda)) - \mathbf{y}_j \theta^\top \mathbf{x}_{ij}(\lambda)] \right\} \right\}.\end{aligned}$$

Notice that

$$\begin{aligned}P(\lambda, B = 1) &= P(B = 1|\lambda)P(\lambda) = \frac{\lambda^\alpha (1-\lambda)^{\beta-1}}{B(\alpha, \beta)} = \frac{\lambda^\alpha (1-\lambda)^{\beta-1}}{B(\alpha+1, \beta)} \times \frac{\alpha}{\alpha+\beta} \\ P(\lambda, B = 0) &= P(B = 0|\lambda)P(\lambda) = \frac{\lambda^{\alpha-1} (1-\lambda)^\beta}{B(\alpha, \beta)} = \frac{\lambda^{\alpha-1} (1-\lambda)^\beta}{B(\alpha, \beta+1)} \times \frac{\beta}{\alpha+\beta}\end{aligned}$$

where $B(\cdot, \cdot)$ is the Beta function. Thus the marginal distribution of B is

$$P(B = 1) = \frac{\alpha}{\alpha+\beta} \quad \text{and} \quad P(B = 0) = \frac{\beta}{\alpha+\beta}$$

and the conditional distribution of λ given B is

$$P(\lambda|B = 1) = \text{Beta}(\alpha+1, \beta) \quad \text{and} \quad P(\lambda|B = 0) = \text{Beta}(\alpha, \beta+1).$$

Then we have

$$\begin{aligned}\mathcal{L}_{mix}(f_\theta, \mathcal{D}) &= \frac{1}{n^2} \sum_{i=1}^n \sum_{j=1}^n \mathbb{E}_B \left\{ \mathbb{E}_{\lambda|B} \left\{ B [h(\theta^\top \mathbf{x}_{ij}(\lambda)) - \mathbf{y}_i \theta^\top \mathbf{x}_{ij}(\lambda)] \right. \right. \\ &\quad \left. \left. + (1-B) [h(\theta^\top \mathbf{x}_{ij}(\lambda)) - \mathbf{y}_j \theta^\top \mathbf{x}_{ij}(\lambda)] \right\} \right\} \\ &= \frac{1}{n^2} \sum_{i=1}^n \sum_{j=1}^n \left\{ \frac{\alpha}{\alpha+\beta} \mathbb{E}_{\lambda \sim \text{Beta}(\alpha+1, \beta)} [h(\theta^\top \mathbf{x}_{ij}(\lambda)) - \mathbf{y}_i \theta^\top \mathbf{x}_{ij}(\lambda)] \right. \\ &\quad \left. + \frac{\beta}{\alpha+\beta} \mathbb{E}_{\lambda \sim \text{Beta}(\alpha, \beta+1)} [h(\theta^\top \mathbf{x}_{ij}(\lambda)) - \mathbf{y}_j \theta^\top \mathbf{x}_{ij}(\lambda)] \right\}.\end{aligned}$$

In addition, let

$$\lambda' = 1 - \lambda \sim \text{Beta}(\beta+1, \alpha).$$

So we can transform the random variable from λ to λ' and have

$$\begin{aligned}\mathbb{E}_{\lambda \sim \text{Beta}(\alpha, \beta+1)} [h(\theta^\top \mathbf{x}_{ij}(\lambda)) - \mathbf{y}_j \theta^\top \mathbf{x}_{ij}(\lambda)] \\ = \mathbb{E}_{\lambda' \sim \text{Beta}(\beta+1, \alpha)} [h(\theta^\top \mathbf{x}_{ji}(\lambda')) - \mathbf{y}_j \theta^\top \mathbf{x}_{ji}(\lambda')].\end{aligned}$$

Plug this equation into $\mathcal{L}_{mix}(f_\theta, \mathcal{D})$,

$$\begin{aligned}\mathcal{L}_{mix}(f_\theta, \mathcal{D}) &= \frac{1}{n^2} \sum_{i=1}^n \sum_{j=1}^n \left\{ \frac{\alpha}{\alpha+\beta} \mathbb{E}_{\lambda \sim \text{Beta}(\alpha+1, \beta)} [h(\theta^\top \mathbf{x}_{ij}(\lambda)) - \mathbf{y}_i \theta^\top \mathbf{x}_{ij}(\lambda)] \right. \\ &\quad \left. + \frac{\beta}{\alpha+\beta} \mathbb{E}_{\lambda \sim \text{Beta}(\beta+1, \alpha)} [h(\theta^\top \mathbf{x}_{ij}(\lambda)) - \mathbf{y}_i \theta^\top \mathbf{x}_{ij}(\lambda)] \right\} \\ &= \frac{1}{n^2} \sum_{i=1}^n \sum_{j=1}^n \mathbb{E}_{\lambda \sim P_\lambda} [h(\theta^\top \mathbf{x}_{ij}(\lambda)) - \mathbf{y}_i \theta^\top \mathbf{x}_{ij}(\lambda)],\end{aligned}$$

where

$$\tilde{P}_\lambda(\lambda) = \frac{\alpha}{\alpha + \beta} \text{Beta}(\alpha + 1, \beta) + \frac{\beta}{\alpha + \beta} \text{Beta}(\beta + 1, \alpha).$$

To proceed further, we denote $P_n(x)$ as the empirical distribution of \mathbf{x} induced by the training sample. Then I_2 can be rewritten as

$$\begin{aligned} \mathcal{L}_{mix}(f_\theta, \mathcal{D}) &= \frac{1}{n} \sum_{i=1}^n \mathbb{E}_{\mathbf{x} \sim P_n} \mathbb{E}_{\lambda \sim \tilde{P}_\lambda} \left[h(\theta^\top (\lambda \mathbf{x}_i + (1 - \lambda) \mathbf{x})) \right. \\ &\quad \left. - \mathbf{y}_i \theta^\top (\lambda \mathbf{x}_i + (1 - \lambda) \mathbf{x}) \right] \\ &= \frac{1}{n} \sum_{i=1}^n \mathbb{E}_{\mathbf{x} \sim P_n} \mathbb{E}_{\lambda \sim \tilde{P}_\lambda} \psi_i(\gamma), \end{aligned}$$

where $\gamma = 1 - \lambda$ and

$$\psi_i(\gamma) = h(\theta^\top ((1 - \gamma) \mathbf{x}_i + \gamma \mathbf{x})) - \mathbf{y}_i \theta^\top ((1 - \gamma) \mathbf{x}_i + \gamma \mathbf{x}).$$

By the second order Taylor expansion,

$$\psi_i(\gamma) = \psi_i(0) + \psi_i'(0)\gamma + \frac{1}{2} \psi_i''(0)\gamma^2 + O(\gamma^3).$$

Furthermore,

$$\begin{aligned} \psi_i'(0) &= h'(\theta^\top \mathbf{x}_i) \theta^\top (\mathbf{x} - \mathbf{x}_i) - \mathbf{y}_i \theta^\top (\mathbf{x} - \mathbf{x}_i) \\ &= (g(\theta^\top \mathbf{x}_i) - \mathbf{y}_i) \theta^\top (\mathbf{x} - \mathbf{x}_i), \end{aligned}$$

and

$$\begin{aligned} \psi_i''(0) &= h''(\theta^\top \mathbf{x}_i) [\theta^\top (\mathbf{x} - \mathbf{x}_i)]^2 \\ &= g(\theta^\top \mathbf{x}_i) (1 - g(\theta^\top \mathbf{x}_i)) [\theta^\top (\mathbf{x} - \mathbf{x}_i)]^2. \end{aligned}$$

Thus we have $\mathcal{L}_{mix}(f_\theta, \mathcal{D}) = \frac{1}{n} \sum_{i=1}^n L(f_\theta(\mathbf{x}_i), \mathbf{y}_i) + I_3 + I_4$, where

$$\begin{aligned} I_3 &= \mathbb{E}_{\lambda \sim \tilde{P}_\lambda} [1 - \lambda] \frac{1}{n} \sum_{i=1}^n \mathbb{E}_{\mathbf{x} \sim P_n} [(g(\theta^\top \mathbf{x}_i) - \mathbf{y}_i) \theta^\top (\mathbf{x} - \mathbf{x}_i)], \\ I_4 &= \mathbb{E}_{\lambda \sim \tilde{P}_\lambda} [(1 - \lambda)^2] \frac{1}{2n} \sum_{i=1}^n \mathbb{E}_{\mathbf{x} \sim P_n} [g(\theta^\top \mathbf{x}_i) (1 - g(\theta^\top \mathbf{x}_i)) [\theta^\top (\mathbf{x} - \mathbf{x}_i)]^2]. \end{aligned}$$

Similarly, for the data $\mathcal{D}_{dis} = \{(\mathbf{x}_i, \mathbf{y}_i^*), \mathbf{y}_i^* = f^T(\mathbf{x}_i), i = 1, \dots, n\}$, the following decomposition also holds: $\mathcal{L}_{mix}(f_\theta, \mathcal{D}_{dis}) = \frac{1}{n} \sum_{i=1}^n L(f_\theta(\mathbf{x}_i), \mathbf{y}_i^*) + I_5 + I_4$, where

$$I_5 = \mathbb{E}_{\lambda \sim \tilde{P}_\lambda} [1 - \lambda] \frac{1}{n} \sum_{i=1}^n \mathbb{E}_{\mathbf{x} \sim P_n} [(g(\theta^\top \mathbf{x}_i) - \mathbf{y}_i^*) \theta^\top (\mathbf{x} - \mathbf{x}_i)].$$

Therefore,

$$\begin{aligned} \mathcal{L}_{mix}(f_\theta, \mathcal{D}) + \alpha \mathcal{L}_{mix}(f_\theta, \mathcal{D}_{dis}) &= \frac{1}{n} \sum_{i=1}^n L(f_\theta(\mathbf{x}_i), \mathbf{y}_i) + \frac{\alpha}{n} \sum_{i=1}^n L(f_\theta(\mathbf{x}_i), \mathbf{y}_i^*) \\ &\quad + (I_3 + \alpha I_5) + (1 + \alpha) I_4. \end{aligned}$$

For the term $I_3 + \alpha I_5$, we have

$$\begin{aligned}
I_3 + \alpha I_5 &= \mathbb{E}_{\lambda \sim \tilde{P}_\lambda} [1 - \lambda] \frac{1}{n} \sum_{i=1}^n ((1 + \alpha)g(\theta^\top \mathbf{x}_i) - \mathbf{y}_i - \alpha \mathbf{y}_i^*) \theta^\top (\mathbb{E}_{\mathbf{x} \sim P_n}(\mathbf{x}) - \mathbf{x}_i) \\
&= \mathbb{E}_{\lambda \sim \tilde{P}_\lambda} [1 - \lambda] \frac{1}{n} \sum_{i=1}^n (\mathbf{y}_i + \alpha \mathbf{y}_i^* - (1 + \alpha)g(\theta^\top \mathbf{x}_i)) \theta^\top \mathbf{x}_i \\
&= \mathbb{E}_{\lambda \sim \tilde{P}_\lambda} [1 - \lambda] \frac{1}{n} \sum_{i=1}^n |\mathbf{y}_i + \alpha \mathbf{y}_i^* - (1 + \alpha)g(\theta^\top \mathbf{x}_i)| \|\theta\|_2 \|\mathbf{x}_i\|_2 \cos(\theta, \mathbf{x}_i) \\
&= \mathbb{E}_{\lambda \sim \tilde{P}_\lambda} [1 - \lambda] \frac{1}{n} \sum_{i=1}^n \left| |\mathbf{y}_i - g(\theta^\top \mathbf{x}_i)| - \alpha |\mathbf{y}_i^* - g(\theta^\top \mathbf{x}_i)| \right| \|\theta\|_2 \|\mathbf{x}_i\|_2 \cos(\theta, \mathbf{x}_i) \\
&\geq R_i c_x \sqrt{d} \mathbb{E}_{\lambda \sim \tilde{P}_\lambda} [1 - \lambda] \frac{1}{n} \sum_{i=1}^n (1 - \alpha k) |\mathbf{y}_i - g(\theta^\top \mathbf{x}_i)| \|\theta\|_2 \\
&\geq \epsilon \sqrt{d} \frac{1}{n} \sum_{i=1}^n (1 + k) |\mathbf{y}_i - g(\theta^\top \mathbf{x}_i)| \|\theta\|_2 \\
&\geq \frac{1}{n} \sum_{i=1}^n \max_{\|\delta_i\|_2 \leq \epsilon \sqrt{d}} (\mathbf{y}_i - g(\theta^\top \mathbf{x}_i)) \theta^\top \delta_i + \frac{\alpha}{n} \sum_{i=1}^n \max_{\|\delta_i\|_2 \leq \epsilon \sqrt{d}} (\mathbf{y}_i^* - g(\theta^\top \mathbf{x}_i)) \theta^\top \delta_i.
\end{aligned}$$

Now we turn to I_4 :

$$\begin{aligned}
I_4 &= \mathbb{E}_{\lambda \sim \tilde{P}_\lambda} [(1 - \lambda)^2] \frac{1}{2n} \sum_{i=1}^n g(\theta^\top \mathbf{x}_i) (1 - g(\theta^\top \mathbf{x}_i)) \theta^\top \mathbb{E}_{\mathbf{x} \sim P_n} [(\mathbf{x} - \mathbf{x}_i)(\mathbf{x} - \mathbf{x}_i)^\top] \theta \\
&= \mathbb{E}_{\lambda \sim \tilde{P}_\lambda} [(1 - \lambda)^2] \frac{1}{2n} \sum_{i=1}^n g(\theta^\top \mathbf{x}_i) (1 - g(\theta^\top \mathbf{x}_i)) \theta^\top (\mathbb{E}_{\mathbf{x} \sim P_n}(\mathbf{x}\mathbf{x}^\top) + \mathbf{x}_i \mathbf{x}_i^\top) \theta \\
&\geq \mathbb{E}_{\lambda \sim \tilde{P}_\lambda} [(1 - \lambda)^2] \frac{1}{2n} \sum_{i=1}^n g(\theta^\top \mathbf{x}_i) (1 - g(\theta^\top \mathbf{x}_i)) \theta^\top \mathbf{x}_i \mathbf{x}_i^\top \theta \\
&= R_i^2 c_x^2 d \mathbb{E}_{\lambda \sim \tilde{P}_\lambda} [(1 - \lambda)^2] \frac{1}{2n} \sum_{i=1}^n g(\theta^\top \mathbf{x}_i) (1 - g(\theta^\top \mathbf{x}_i)) \|\theta\|_2^2 \\
&\geq \epsilon^2 d \frac{1}{2n} \sum_{i=1}^n g(\theta^\top \mathbf{x}_i) (1 - g(\theta^\top \mathbf{x}_i)) \|\theta\|_2^2 \\
&= \frac{1}{n} \sum_{i=1}^n \max_{\|\delta_i\|_2 \leq \epsilon \sqrt{d}} g(\theta^\top \mathbf{x}_i) (1 - g(\theta^\top \mathbf{x}_i)) (\theta^\top \delta_i)^2.
\end{aligned}$$

Combining the results of $I_3 + \alpha I_5$ and I_4 , we know that $I_3 + \alpha I_5 \geq I_1 + \alpha I_2$. Furthermore, we have

$$\tilde{\mathcal{L}}(f_\theta, \mathcal{D}) + \alpha \tilde{\mathcal{L}}(f_\theta, \mathcal{D}_{dis}) \leq \mathcal{L}_{mix}(f_\theta, \mathcal{D}) + \alpha \mathcal{L}_{mix}(f_\theta, \mathcal{D}_{dis}).$$

□

Next we extend the above theorem to the case of neural networks with ReLU activation and max-pooling. We still consider the binary classification task with the logistic loss and take $f_\theta(x)$ to be a fully connected neural network with ReLU activation function or max-pooling:

$$f_\theta(x) = \mathbf{a}^\top \sigma(W_{N-1} \cdots \sigma(W_2 \sigma(W_1 x))),$$

where $\sigma(\cdot)$ is a nonlinear function that consists of ReLU activation and max pooling, each W_i is a matrix, and \mathbf{a} is a column vector: i.e., θ consists of $\{W_i, i = 1, \dots, W - 1\}$ and \mathbf{a} . According to the derivatives of ReLU and max-pooling, the function f_θ satisfies that $\nabla_x^2 f_\theta(x) = 0$ and $f_\theta(x) = \nabla_x f_\theta(x)^\top x$ almost everywhere. Therefore a fully connected neural networks with ReLU activation functions and max-pooling can be locally approximated by a linear function. By the results of logistic regression, we have the following theorem:

Theorem. Suppose $f_\theta(x) = \nabla_x f_\theta(x)^\top x$, $\nabla_x^2 f_\theta(x) = 0$ and there exists a constant $c_x > 0$ such that $\|\mathbf{x}_i\|_2 > c_x \sqrt{d}$ for all $i \in \{1, \dots, n\}$. Then, for any $\theta \in \Theta$, we have

$$\tilde{\mathcal{L}}(f_\theta, \mathcal{D}) + \alpha \tilde{\mathcal{L}}(f_\theta, \mathcal{D}_{dis}) \leq \mathcal{L}_{mix}(f_\theta, \mathcal{D}) + \alpha \mathcal{L}_{mix}(f_\theta, \mathcal{D}_{dis}),$$

where the size of the adversarial attack ϵ is

$$\epsilon = \frac{1 - \alpha\beta}{1 + \beta} c_x R \mathbb{E}_{\lambda \sim \tilde{P}_\lambda} [1 - \lambda], \quad \text{with} \quad R = \min_{i \in \{1, \dots, n\}} |\cos(\nabla_x f_\theta(x), \mathbf{x}_i)|,$$

and the distribution \tilde{P}_λ is

$$\tilde{P}_\lambda(\lambda) = \frac{\alpha}{\alpha + \beta} \mathbf{Beta}(\alpha + 1, \beta) + \frac{\beta}{\alpha + \beta} \mathbf{Beta}(\beta + 1, \alpha).$$

□